IFNα Inhibits JAK2V617F-Driven Neoplastic Vasculogenesis and Endothelial-to-Mesenchymal Transition in a 3D iPSC-Based Bone Marrow Niche Model

Madeline J. Caduc[1,2], Mohamed H. E. Mabrouk[3], Cristina B. Lopez[1,2], Martin Grasshoff[4], Eva M. Buhl[5], Sabrina Ernst[6], Dickson W. L. Wong[5], Gerhard Müller-Newen[7], Michael Vogt[8], Jörg Eschweiler[9,10], Peter Boor[5], Maximilian Ackermann[5], Nicolas Chatain[1,2], Julia Franzen[3], Ivan G. Costa[4], Martin Zenke[1], Rebekka K. Schneider[11], Tim H. Brümmendorf[1,2], Steffen Koschmieder[1,2,12*], Marcelo A. S. de Toledo[1,2,12*]

1 Department of Hematology, Oncology, Hemostaseology and Stem Cell Transplantation, Faculty of Medicine, RWTH Aachen University, Aachen, Germany

2 Center for Integrated Oncology Aachen Bonn Cologne Düsseldorf (CIO ABCD), Aachen, Germany

3 Genomics Facility, Interdisciplinary Center for Clinical Research IZKF, RWTH Aachen University, Aachen, Germany

4 Institute for Computational Genomics, RWTH Aachen University, Aachen, Germany

5 Institute of Pathology and Electron Microscopy Facility, RWTH Aachen University Hospital, Aachen, Germany

6 Confocal Microscopy Facility, Interdisciplinary Center for Clinical Research IZKF, Uniklinik RWTH Aachen, Aachen, Germany

7 Institute of Biochemistry and Molecular Biology, Uniklinik RWTH Aachen, Aachen, Germany

8 Two-Photon Imaging Facility, Interdisciplinary Center for Clinical Research IZKF, RWTH Aachen University Hospital, Aachen, Germany

9 Department of Trauma and Reconstructive Surgery, Faculty of Medicine, Martin-Luther-University Halle (Saale), Germany

10 Department of Trauma and Reconstructive Surgery, BG Klinikum Bergmannstrost Halle (Saale), Germany

11 Institute for Cell and Tumor Biology, RWTH Aachen University, Aachen, Germany

12 shared senior authorship

* Corresponding authors: Dr. Marcelo A. S. de Toledo, PhD, and Prof. Dr. med. Steffen Koschmieder, Department of Hematology, Oncology, Hemostaseology, and Stem Cell Transplantation, Faculty of Medicine, RWTH Aachen University, Pauwelsstr. 30, D-52074 Aachen, Germany, Phone: +49-241-8036102; E-mail: mszymanskide@ukaachen.de and skoschmieder@ukaachen.de

Abstract

The vascular niche plays a crucial role in regulating hematopoiesis, and the presence of JAK2V617F endothelial cells (EC) in myeloproliferative neoplasms (MPN) underscores its therapeutic significance. Leveraging patient-specific induced pluripotent stem cells (iPSC) harboring JAK2^{WT} or the MPN-driver JAK2V617F (heterozygous, JAK2V617F^{HET} or homozygous, JAK2V617F^{HOM}), we developed a scalable 3D bone marrow (BM)-niche mimicking model to study neoplastic vasculogenesis with precise control over cellularity and genetics. Global RNA-sequencing revealed zygosity-dependent phenotypic differences in EC, with JAK2V617F^{HET} iPSC-derived EC (iEC) shifting toward a pro-mesenchymal phenotype via endothelial-to-mesenchymal transition (EndMT), while JAK2V617F^{HOM} iEC displayed dysregulated translation machinery. EndMT was exacerbated in JAK2V617F^{HET} iEC-mesenchymal stromal cells 3D cocultures exposed to inflammatory cytokines and was effectively inhibited by the tyrosine kinase inhibitors ruxolitinib and nintedanib. Notably, interferon-alpha (IFNα) showed potential in reducing EndMT, with its anti-EndMT effect validated *in vivo* in murine and MPN patient samples. Single-cell RNA sequencing revealed that JAK2V617F hematopoietic cells further amplified EndMT, emphasizing the interplay between the vascular niche and hematopoietic compartments. To our knowledge, this is the first study to report that IFNα's anti-fibrotic and anti-angiogenic effects may be partly mediated through EndMT inhibition. Our 3D coculture model offers a powerful platform for mechanistic studies of human hematopoiesis.

Introduction

Myelofibrosis (MF) is a late-stage subtype of BCR-ABL1-negative myeloproliferative neoplasms (MPN), characterized by progressive bone marrow (BM) fibrosis leading to loss of support of normal hematopoiesis, alongside inflammatory and vascular complications[1]. Thrombotic events often precede MPN diagnosis, with patients carrying JAK2V617F being at higher risk[2]. Moreover, perturbations in the vascular niche, such as aberrant neoangiogenesis[3,4] and endothelial dysfunction through endothelial-to-mesenchymal-transition (EndMT)[5], influence MPN progression by modulating hematopoietic stem cell homeostasis and therapeutic outcomes[6,7]. While the precise origin of MPN remains debated, recent studies and the presence of JAK2V617F endothelial cells (EC) in MPN patients support the hypothesis that these clonal hematological malignancies may arise from a common precursor cell, the hemangioblast[8–11].

Among the approved therapies with disease-modifying potential in MPN, interferon-alpha (IFNα) induces hematologic and molecular responses, potentially reducing vascular complications and fibrotic progression[12,13]. In addition to directly impacting cancer cell proliferation and promoting adaptive immune responses, IFNα also mediates antitumor effects by inhibiting angiogenesis[14]. Previous studies have explored IFNα's transcriptional signature in EC[15], but its impact on the malignant clone microenvironment and JAK2V617F+ vascular niche remains to be elucidated.

Since the advent of induced pluripotent stem cell (iPSC) technology, human iPSC have been extensively used for 2D *in vitro* assays[16]. However, the BM is a highly specialized and complex tissue where the spatial organization within specific niches tightly regulates hematopoiesis[17]. *In vivo*, stress conditions such as inflammation or drug treatments may affect niche components differently than in isolated 2D *in vitro* environments. Thus, establishing 3D models that replicate the organization of key BM

109 niche components is essential for more translationally relevant preclinical research and
110 drug development, potentially reducing reliance on animal testing.

111 In this study, global transcriptomic analysis of iPSC-derived EC (iEC) revealed
112 zygosity-specific transcriptional signatures, with heterozygous JAK2V617F iEC
113 (JAK2V617F^{HET}) showing a bias toward EndMT, while homozygous iEC
114 (JAK2V617F^{HOM}) exhibited dysregulated translation machinery. 3D cocultures,
115 combining iEC with mesenchymal stromal cells (MSC), successfully replicated critical
116 EC-pericyte interactions necessary for blood vessel formation[18]. Single-cell RNA
117 sequencing (scRNA-seq) of 3D cocultures incorporating iEC, MSC, and iPSC-derived
118 hematopoietic cells (iHC) captured key cellular interactions within the neoplastic BM
119 niche, providing novel evidence that the anti-fibrotic potential of IFNα may rely on its
120 anti-EndMT properties. IFNα's anti-EndMT effect was validated *in vivo* using BM
121 samples from a murine MPN model driven by TPO overexpression and MPN patients.
122 Thus, our innovative 3D *ex vivo* model provides a valuable platform for unraveling the
123 complex cellular interactions underlying MF pathogenesis and evaluating the impact of
124 therapeutic interventions, such as IFNα, on the BM niche.

125

126 ## Methods

127 ### Ethics Approval and Consent to Participate

128 Peripheral blood mononuclear cells (PBMC) from MPN patients were obtained from
129 the centralized Biomaterial Bank of the Faculty of Medicine, RWTH Aachen University
130 Hospital. The primary MSC used in this study were isolated from the femoral heads of
131 patients undergoing hip replacement surgery (Department of Orthopaedics, Trauma
132 and Reconstructive Surgery, Faculty of Medicine, RWTH Aachen University). All
133 biological samples were obtained with written informed consent, as approved by the
134 Ethics Committee of the RWTH Aachen University [EK206/09, EK127/12, EK300/13].

135 **Differentiation of MPN Patient-Specific iPSC Towards Endothelial and**
136 **Hematopoietic Lineages**

137 The iPSC lines used in the present study were previously characterized[19,20] and are
138 listed in the Supplementary Table 1. A description of the endothelial and hematopoietic
139 differentiation protocol and culture methods is provided in the Supplementary Methods.
140

141 **Modeling Vasculogenesis in 3D Fibrin-Based Hydrogels**

142 Fibrin hydrogels were generated based on an adapted protocol as previously
143 described[21]. The composition of fibrin hydrogels is detailed in Supplementary Table 2.
144 After enzymatic harvesting, MSC and/or iEC were suspended in Endothelial Basal
145 Medium 2 (EBM2, Lonza) at the desired density (MSC: iEC $6x10^4$: $2x10^4$ cells). The
146 cell suspension was then mixed with aprotinin (500 µg/ml, Sigma Aldrich) and thrombin
147 (2,5 U/ml, Sigma Aldrich), followed by the addition of fibrinogen (5 mg/ml, Merck).
148 Following polymerization, the generated constructs were immersed in Endothelial
149 Growth Medium 2 (EGM2, Lonza) and cultured under submerged conditions in a
150 controlled incubator environment for up to 5 days, with half-medium changes
151 performed every 48 hours.
152

153 **3D Modeling of Endothelial-to-Mesenchymal Transition**

154 After being incubated in EGM2 for 48 hours to foster the formation of vascular
155 networks, the 3D MSC-iEC cocultures underwent a 4-hour pre-incubation period in
156 starvation medium (EBM2 + 2% FCS). To explore the anti-EndMT potential of selected
157 drugs, starvation medium was supplemented with either 1000 U/ml IFNα, 250 nM
158 ruxolitinib, 250 nM nintedanib, or a combination of ruxolitinib and nintedanib (both at
159 250 nM). EndMT was then induced by adding a cocktail of proinflammatory cytokines
160 including transforming growth factor (TGF)-β (0.5 ng/ml), interleukin (IL)-1β (5 ng/ml),

161 and tumor necrosis factor (TNF)-α (10 ng/ml). Negative controls were maintained in
162 starvation medium. After 48 hours, the 3D constructs were fixed in 4% PFA before
163 being processed for paraffin embedding. Immunofluorescence staining was performed
164 to assess protein levels of different key EndMT markers (Supplementary Table 3).
165

166 **Generation of 3D iPSC-Based Cocultures for Single-Cell RNA Sequencing**

167 For scRNA-seq, 3D cocultures containing MSC, iEC, and iHC were generated. iHC
168 included hematopoietic stem and progenitor cells (iHSPC), megakaryocytes (iMK),
169 monocytes/macrophages (iM), and granulocytes (iGr). Following harvesting, the cells
170 were suspended in fibrin hydrogels at the desired cell density (MSC: iEC: iHC ratio of
171 $6x10^4$: $2x10^4$: $12x10^4$ cells).
172 Additional information regarding the different 3D experimental setups utilized in the
173 present study can be found in the Supplementary Methods.
174

175 **Statistical Analysis**

176 Graphical display and statistical analysis were performed with Prism (GraphPad, San
177 Diego, CA, USA). P values of <0.05 were considered statistically significant. Results
178 are presented as mean ± standard of deviation. (*p < 0.05, **p < 0.01, ***p < 0.001).
179

180 **Additional Experimental Procedures**

181 The Supplementary Methods provide detailed methods for iPSC differentiation,
182 generating 3D iPSC-based cocultures, proliferation and apoptosis assay, *in vitro* drug
183 screening, confocal and transmission electron microscopy, validation experiments
184 using murine and human BM trephines, as well as protocols for immunofluorescence,
185 flow cytometry, RNA sequencing (global and scRNA-seq), RT-qPCR, and associated
186 reagents, including primers (Supplementary Table 4), FACS antibodies

187 (Supplementary Table 5), compounds (Supplementary Table 6), and media
188 compositions.
189

190 ## Results

191 **IFNα Exerts Anti-Angiogenic Effects Without Direct Vascular Toxicity on iPSC-**
192 **Derived Endothelial Cells**

193 To elucidate the effects of JAK2V617F on human vasculogenesis, we leveraged
194 high-purity and clonal patient-specific $JAK2^{WT}$, $JAK2V617F^{HET}$, and $JAK2V617F^{HOM}$
195 iEC (Supplementary Fig.1A, Supplementary Table 1). Following endothelial
196 differentiation and CD144+ magnetic-activated cell sorting, iEC purity was above
197 97.13±3.27% (CD31+CD144+CD105+ cells), as determined by flow cytometry
198 analysis (FACS). Importantly, JAK2V617F zygosity did not impact endothelial
199 differentiation (Supplementary Fig. 1B). The generated iEC featured a classical flat,
200 cobblestone endothelial morphology (Fig. 1A). However, mutated iEC showed an
201 increased proliferation rate in comparison to unmutated cells (Fig. 1B). To assess the
202 capacity for vascular network formation across different iEC genotypes, we performed
203 endothelial tube formation assays (ETFA). iEC were able to form capillary-like
204 structures, with no significant differences observed between the 3 genotypes (Fig. 1C-
205 D). These results suggest that JAK2V617F does not impact EC differentiation or
206 angiogenic potential but provides a proliferative advantage to EC.

207 Although vascular niche dysregulation is increasingly recognized as pivotal in
208 MPN progression to MF[7], the impact of clinically used MPN therapies on the
209 endothelium remains poorly understood. Thus, we investigated the vascular toxicity of
210 drugs currently used or under investigation for MPN treatment. Treatment with 1 μM of
211 fedratinib, venetoclax, and anagrelide reduced iEC viability. However, no significant

alterations were observed upon exposure to 1 μM of hydroxyurea, ruxolitinib, AMG232 or 1000 U/ml IFNα (Fig. 1E), suggesting a favorable vascular toxicity profile.

To assess IFNα's anti-angiogenic potential, we then performed ETFA. Exposure to 1000 U/ml IFNα did not alter iEC capillary-like structure formation (Supplementary Fig. 1C), but pre-sensitizing of iEC with 1000 U/ml IFNα significantly impaired their angiogenic potential (Fig. 1F-H). Subsequent treatment with 1000 U/ml IFNα did not increase the observed anti-angiogenic effect (Supplementary Fig. 1D). Overall, no genotype-specific differences were observed, suggesting a genotype-independent mechanism.

IFNα Impairs Neoplastic Vasculogenesis in a 3D iPSC-Based Model

To better model the impact of JAK2V617F on the three-dimensional formation of vessel-like structures, we developed an adaptive 3D fibrin-based system that replicates the essential homotypic and heterotypic interactions between EC and MSC, required for blood vessel formation. Based on recent studies underscoring the ability of MSC to differentiate into pericytes[22], MSC and iEC were suspended either as mono- or cocultures within fibrin hydrogels (Fig. 2A). Confocal microscopy revealed MSC alignment along the wall of formed tubule-like structures, mirroring the EC-pericyte arrangement *in vivo* (Fig. 2B). Transmission electron microscopy (TEM) analysis confirmed iEC arrangement into vessel-like structures with the presence of lumina lined by iEC and abluminal deposition of extracellular matrix (ECM) components (Supplementary Fig. 1E). While iEC self-assembled into tubule-like structures in monocultures, coculture with MSC resulted in a significantly augmented network area (Fig. 2C-D), suggesting a supportive role of MSC for vascular tree formation. Similarly to the previous ETFA results, no differences were observed between the genotypes (Supplementary Fig. 1F).

238 Interestingly, while the increased vascular network formation was not altered by
239 acute IFNα treatment (Fig. 2D), separate pre-sensitizing of iEC and MSC prior to 3D-
240 cocultivation, significantly impaired vascular tree formation (Fig. 2E-F).
241 Thus, our model serves as a valuable platform for investigating vasculogenesis *in vitro*,
242 emphasizing the anti-angiogenic effects of IFNα.
243

244 **JAK2V617F^{HET} iEC Exhibit a Pro-Mesenchymal Phenotype while JAK2V617F^{HOM}**
245 **iEC Display Dysregulated Translation Machinery**

246 To further investigate the impact of JAK2V617F on the endothelium, we
247 performed global transcriptomic analysis (RNAseq) of JAK2^{WT} and mutated iEC
248 (Supplementary Table 7). iEC exhibited a high cosine similarity to primary human EC
249 but not to unrelated cells, and, consistent with previous research[23], displayed a
250 vascular transcriptional signature (Supplementary Fig. 2A, Supplementary Table 8).
251 Unsupervised hierarchical clustering of differentially expressed genes (DEG)
252 effectively grouped samples by JAK2V617F zygosity (Fig. 3A), with comparable
253 expression of JAK2 and STAT1 across genotypes (Supplementary Fig. 2B). Differential
254 gene expression analysis revealed zygosity-specific transcriptional dysregulations with
255 potentially significant implications for EC properties.

256 JAK2V617F^{HET} iEC exhibited upregulation of pathways related to mesenchymal
257 development, ECM synthesis, and organization (Supplementary Fig. 2C). Kyoto
258 Encyclopedia of Genes and Genomes (KEGG) pathway enrichment analysis further
259 highlighted increased expression of genes involved in cell adhesion molecules
260 (Supplementary Fig. 2D). Gene set enrichment analysis (GSEA) revealed significant
261 upregulation of the TGFβ signaling pathway and genes associated with epithelial-to-
262 mesenchymal transition (EMT) (Fig. 3B). Although aberrant neoangiogenesis is a
263 recognized contributor to MF pathogenesis, approximately 30% of BM EC in MF

264 patients have been reported to display a mesenchymal phenotype, suggesting
265 EndMT[5]. Consistent with this transcriptional profile, key EndMT markers, including
266 fibroblast-specific protein 1 (*FSP1*) and alpha-smooth muscle actin (*ACTA2*), were
267 upregulated in JAK2V617F$^{HET\ vs.\ WT}$, as confirmed by RT-qPCR (Fig. 3C)[24]. Additionally,
268 GSEA identified enrichment of genes related to hypoxia and reactive oxygen species
269 (ROS) pathways, both of which are critical in MPN pathogenesis[25,26]. Further
270 statistically enriched gene sets from the MSigDB Hallmark collection are presented in
271 Supplementary Fig. 2E.

272 Ribosome biogenesis is a key factor in carcinogenesis, and recent studies have
273 suggested that impaired ribosomal protein function may contribute to defective
274 hematopoiesis and MF[27]. Notably, GSEA revealed a downregulation of genes related
275 to translation and ribosome function in JAK2V617F^{HOM} iEC (Fig. 3D). In parallel, Gene
276 Ontology (GO) enrichment analysis highlighted significant disruptions in the translation
277 machinery, including downregulation of terms associated with ribosome biogenesis,
278 ribonucleoprotein complex assembly, and RNA splicing (Supplementary Fig. 3A). TEM
279 revealed disorganized endoplasmic reticulum (ER)-ribosome structures, leading to a
280 marked reduction in rough ER (rER) in JAK2V617F^{HOM} iEC (Fig. 3E, Supplementary
281 Fig. 3B-C). Additionally, we observed significant transcriptional downregulation of non-
282 coding RNA (ncRNA) involved in regulating the translation machinery, including
283 *SNORA73B*, *RNY3*, *RNU11* and *RNU5E-1* (Supplementary Fig. 3D)[28–30].

284 Altogether, our results indicate zygosity-specific dysregulations in iEC:
285 JAK2V617F^{HET} iEC exhibit a shift towards a pro-mesenchymal phenotype, whereas
286 JAK2V617F^{HOM} iEC show disruptions in the translation machinery.

287

288

289 **IFNα Treatment Elicits Genotype-Specific Transcriptional Signatures in MPN-**
290 **Patient iEC**

291 Next, we extended our analysis to investigate the genotype-specific
292 transcriptional response of iEC to IFNα treatment. Principal component analysis (PCA)
293 analysis effectively grouped samples by treatment and JAK2V617F-zygosity
294 (Supplementary Fig. 4A). Following IFNα treatment, iEC exhibited a robust core IFNα
295 response (Fig. 4A), characterized by the upregulation of pathways associated with
296 antiviral and immune-modulatory effects (Fig. 4B), among which *IFIT1*, *STAT1*, and
297 *USP18* were additionally confirmed using RT-qPCR (Supplementary Fig. 4B).
298 Importantly, IFNα treatment did not induce apoptosis, as evidenced by Annexin V/7-
299 amino-actinomycin (annexin V/7-AAD) staining and FACS analysis (Supplementary
300 Fig. 4C–E). This observation aligns with our initial drug screening assay, where 72-
301 hour IFNα treatment did not reduce iEC viability (Fig. 1E).

302 Pathway responsive genes (PROGENy) analysis displayed a strong JAK-STAT
303 signaling increase upon IFNα treatment, with no differences across the 3 genotypes
304 (Fig. 4C). Analysis of DEG following IFNα treatment revealed a genotype-specific
305 transcriptional signature (Fig. 4D, Supplementary Fig. 4F). Interestingly,
306 JAK2V617F^{HOM} iEC exhibited the highest number of specific DEG (WT: 29, HET: 13,
307 HOM: 43; Supplementary Table 9), including upregulation of ncRNA involved in
308 translation machinery, such as *RNU12*, along with *RNY3* and *RNU5E-1*, previously
309 downregulated compared to WT controls (Fig. 4E, Supplementary Fig. 3D)[31,32]. This
310 pattern was absent in JAK2^{WT} iEC treated with IFNα (Supplementary Fig. 4G).
311 Selected ncRNA were validated by RT-qPCR (Supplementary Fig. 4H). Furthermore,
312 GO analysis of DEG enriched in JAK2V617F^{HOM} iEC revealed upregulation of
313 pathways related to ribosome biogenesis and mRNA splicing, indicating a potential
314 impact of IFNα on the translation machinery. (Fig. 4F).

315 Our findings underscore JAK2V617F zygosity-specific transcriptional signatures
316 following IFNα treatment, suggesting distinct mechanisms through which IFNα may
317 directly influence the mutant vascular niche properties.
318

319 **IFNα and Tyrosine Kinase Inhibitors Mitigate the Pro-Fibrotic Phenotype of**
320 **JAK2V617F^{HET} iEC**

321 Given the pro-mesenchymal transcriptional signature observed in
322 JAK2V617F^{HET} iEC, we further investigated the contribution of the mutated vascular
323 network to the BM niche fibrotic transformation in 3D cocultures (Fig. 5A). Exposure of
324 3D MSC-iEC cocultures to pro-inflammatory and pro-fibrotic stimuli (TGFβ, IL-1β, and
325 TNFα) recapitulated the changes observed in MPN during myelofibrotic
326 transformation, evidenced by increased deposition of collagen 1 (Col1a1) and alpha
327 smooth muscle actin (αSMA) (Supplementary Fig. 5A-B). Notably, increased FSP1
328 protein expression was observed in JAK2V617F^{HET} iEC-based cocultures under both
329 basal conditions and following cytokine exposure, in comparison to unmutated
330 cocultures (Fig. 5B-C). CD31-FSP1 colocalization analysis unveiled a more
331 pronounced FSP1 protein expression in JAK2V617F^{HET} iEC compared to their WT
332 control following cytokine exposure (Fig. 5D-E). The acquisition of a mesenchymal
333 phenotype by iEC upon cytokine stimulation was confirmed in a 2D *in vitro* setting, with
334 the transcriptional upregulation of Snail homolog 1 (*SNAI1*) and concomitant
335 downregulation of *CD31* (Supplementary Fig. 5C). Consistent with our previous
336 RNAseq, JAK2V617F^{HET} iEC displayed lower Claudin 5 (*CLDN5*) mRNA levels
337 following cytokine exposure compared to JAK2^{WT} iEC (Supplementary Fig. 5C).

338 EndMT, a pivotal process driving fibrosis, facilitates the transition of EC toward
339 mesenchymal and pro-fibrotic phenotypes, contributing to disease progression in
340 fibrotic disorders. While tyrosine kinase inhibitors (TKI) like ruxolitinib and nintedanib

341 have demonstrated anti-fibrotic properties, including suppression of EndMT[33–35], the
342 mechanisms underlying IFNα's disease-modifying effects remain unclear[12,13]. To
343 address this gap, we investigated whether therapeutic intervention with IFNα could
344 mitigate EndMT in our 3D cocultures. Ruxolitinib was used as a positive control, while
345 nintedanib was evaluated both as a standalone treatment and in combination with
346 ruxolitinib to assess potential synergistic effects, given its emerging relevance in
347 hematologic malignancies[36] (Fig. 5A). Pre-sensitizing iEC–MSC 3D cocultures with
348 IFNα (1000 U/mL), nintedanib (250 nM), ruxolitinib (250 nM), or their combination (250
349 nM each) did not significantly alter CD31 expression, except in JAK2V617F^{HET}
350 cocultures, where IFNα treatment increased CD31 fluorescence area (Supplementary
351 Fig. 6A-B). IFNα exhibited a trend toward reducing FSP1 protein levels, while
352 nintedanib, ruxolitinib, and their combination significantly lowered both overall and iEC-
353 specific FSP1 levels in JAK2^{WT} and JAK2V617F^{HET} 3D cocultures (Fig. 5F,
354 Supplementary Fig. 6A, C). This reduction was accompanied by decreased expression
355 of Col1a1 and αSMA (Supplementary Fig. 6D-E). Collectively, these results suggest
356 that while IFNα shows potential in inhibiting EndMT, ruxolitinib and nintedanib exhibit
357 greater efficacy as single treatments.

358 To validate the observed anti-EndMT effect of IFNα *in vivo*, we performed FSP1
359 staining on BM sections from a murine MPN model driven by TPO overexpression and
360 characterized by pronounced dysplastic megakaryopoiesis with strong BM fibrosis and
361 splenomegaly[37]. We observed a significant FSP1 upregulation in the BM of diseased
362 animals (TPO-overexpression group) as compared to control animals (empty vector
363 (EV) group), both globally and within the vascular niche. Notably, FSP1 protein
364 upregulation was completely reversed by IFNα *in vivo* treatment (Fig. 6A-C). These *in*
365 *vivo* findings in mice were further corroborated using primary human BM samples from
366 patients treated with pegylated IFNα as part of their routine MPN treatment, and these

367 analyses also demonstrated a significant reduction in FSP1 upon IFNα treatment (Fig.
368 6D-E).

369 Thus, the results from our *in vitro* 3D iEC-MSC coculture model were confirmed
370 *in vivo*, demonstrating that IFNα modulates the malignant clone microenvironment
371 through EndMT inhibition.

372

373 **3D iPSC-Based Complex Cocultures Mimic Key Cellular Interactions of the**
374 **Human BM Niche**

375 To better replicate *in vivo* conditions, we enhanced our 3D cocultures by
376 incorporating $JAK2^{WT}$ or $JAK2V617F^{HET}$ iHC into the iEC-MSC cocultures, creating 3D
377 MPN BM niches that model human neoplastic vasculogenesis and hematopoiesis.
378 These complex cocultures were generated by combining iEC and MSC with iPSC-
379 derived hematopoietic cells, including hematopoietic stem/progenitor cells (iHSPC,
380 $CD117^{+}CD34^{+}$), megakaryocytes (iMK, $CD45^{+}CD61/41^{+}$), monocytes/macrophages
381 (iM, $CD45^{+}CD68^{+}$), and granulocytes (iGr, $CD45^{+}CD66b^{+}$) (collectively termed iHC)
382 (Fig. 7A, Supplementary Fig. 7A). Following 5 days of *in vitro* 3D coculture, scRNAseq
383 was performed to investigate JAK2V617F-driven transcriptional changes, with a
384 particular emphasis on the effects of JAK2V617F in EC alone versus both endothelial
385 and hematopoietic cells.

386 Distinct hematopoietic populations, predominantly of the myeloid lineage, were
387 identified based on their transcriptional profiles and key marker expression (Fig. 7B).
388 The genes used for cell cluster annotation are listed in Supplementary Table 10. Within
389 the non-hematopoietic ($CD45^{-}$) lineage, we identified 8 distinct cell clusters: 6
390 mesenchymal, 1 endothelial, and 1 hemogenic endothelial (Supplementary Fig.7B).
391 Among the mesenchymal clusters, 3 clusters (0, 1, 2) displayed a "core" mesenchymal
392 signature with high expression of *LEPR*, *NES*, *PDGFRA*, *PDGFRB*, and

393 hematopoiesis-supporting factors such as *CXCL12*, *SCF*, and *ANGPT1*. Cluster 3
394 showed increased *NES* expression but reduced PDGFRs and hematopoietic support
395 genes, except *CXCL12*. Cluster 6 exhibited a similar signature as cluster 3 but showed
396 marked proliferation, as indicated by the higher proportion of cells in the G2/S cell cycle
397 phase. Cluster 7 exhibited a pericyte signature with high expression of *PDGFRB*,
398 *ACTA2*, *ANGPT1*, and *MCAM*. In the endothelial lineage, cluster 5 had a hemogenic
399 endothelial signature and cluster 4 displayed high expression of key endothelial
400 markers such as *CLDN5*, *CDH5* (CD144), *PECAM1*, *KDR* (VEGFR2), and *FLT1*
401 (VEGFR1). Consistent with the vascular transcriptional signature identified in the iEC
402 monoculture RNA-seq analysis (Supplementary Table 8), the EC cluster exhibited
403 elevated expression of arterial markers such as *DLL4* and *CXCR4*.

404 Next, we investigated intercellular signaling between distinct cellular
405 compartments by conducting a crosstalk analysis of scRNAseq data from unmutated
406 3D complex cocultures. This analysis revealed intricate autocrine and paracrine
407 interactions between the hematopoietic and stromal compartments (Fig. 7C). Mapping
408 the expression of interacting ligand-receptor (L-R) pairs identified the stromal
409 compartment and basophil progenitors as the primary sources of outgoing signals,
410 engaging extensively in autocrine and paracrine communication via ECM components
411 (e.g., collagen, laminin) and growth factors (e.g., VEGF, PDGF, KIT) (Fig. 7D). The
412 predicted L-R communication network between the stromal and hematopoietic
413 compartments included key regulatory mediators such as ANGPT1/2–TEK, KIT–KITL,
414 CXCL12–CXCR4, and JAG1–NOTCH1, highlighting the stromal compartment's critical
415 role in maintaining the structural and functional integrity of the BM niche
416 (Supplementary Fig. 7C-D).

417

418

419 **JAK2V617F 3D iPSC-Based Complex Cocultures Capture MPN Key Features**

420 We then assessed the ability of our 3D model to replicate key features of MPN.
421 PROGENy analysis revealed that JAK2V617F in both the endothelial and
422 hematopoietic lineages within our 3D BM niche model significantly upregulated hypoxic
423 signaling (Fig. 8A). As a central hallmark of MPN, this pathway plays a pivotal role in
424 promoting disease progression and shaping therapeutic responses[26]. In addition,
425 critical cell types involved in fibrotic processes, such as monocytes/macrophages,
426 neutrophils, MSC, dendritic cells, and mast cells[36,38,39], exhibited substantial activation
427 of the pro-inflammatory JAK-STAT pathway. The TGFβ pathway, which plays a critical
428 role in tissue fibrosis[40], was activated in various MSC populations, mast cells, and
429 monocytes (Fig. 8A). Interestingly, we observed a significant downregulation of IFNα
430 and TNFα signaling in MSC populations (clusters 1, 5, and 6), while monocytes (cluster
431 0), mast cells (clusters 2 and 7), eosinophils (clusters 4 and 14), neutrophils (clusters
432 8 and 9), and dendritic cells (cluster 12) displayed enriched IFNα signaling (Fig. 8A).

433 Given the prominent role of the mesenchymal compartment in fibrosis, we
434 further examined the differential activation of key signaling pathways within the CD45-
435 lineage. The mesenchymal subclusters exhibited heterogeneous signaling patterns,
436 consistent with the previously documented complexity of the human BM stromal
437 niche[38]. Notably, we observed upregulation of pathways associated with fibrosis and
438 carcinogenesis, such as MAPK and PI3K, in pericytes (cluster 7) and MSC (clusters 6
439 and 2) (Supplementary Fig. 8A). Additionally, pathway activity analysis revealed
440 differential upregulation of the TGFβ pathway and ECM-related gene sets in MSC
441 populations (Supplementary Fig. 8B).

442 While the roles of various MSC subsets in MF have been previously
443 explored[38,41], the intricate L-R interactions and signaling pathways driving fibrosis
444 remain poorly understood. Our analysis of L-R pair expression revealed heightened

445 cellular crosstalk in JAK2V617F^{HET} cocultures compared to WT controls, with aberrant
446 signaling primarily originating from basophil progenitors and stromal compartments,
447 including pericytes, stromal cells, and EC. This enhanced communication involved
448 ECM components (e.g., laminin, collagen, FN1), angiogenic factors (e.g., PDGF,
449 VEGF, ANGPTL), and inflammatory mediators (e.g., TGFβ) (Fig. 8B-C). Additionally,
450 we identified increased interactions between hemogenic endothelium/stem cells,
451 hematopoietic progenitors, megakaryocytes, and EC with basophil progenitors via the
452 pro-inflammatory MIF-CD74 axis (Supplementary Fig. 8C), a pathway implicated in
453 MPN development[42]. Notably, our findings align with recent studies describing a
454 feedback loop in which expanded basophils, mast cells, megakaryocytes, and stromal
455 cell subsets establish a self-reinforcing pro-inflammatory niche and upregulate
456 galectin-1 (*LGALS1*) expression[43]. In JAK2V617F^{HET} cocultures, basophil progenitors
457 exhibited increased autocrine and paracrine signaling with megakaryocytes and
458 monocytes through the LGALS1-ITGB1 axis (Supplementary Fig. 8D)
459 Thus, our 3D complex cocultures effectively mimic key features of MPN and
460 serve as a valuable tool for mechanistic studies of human malignant hematopoiesis.
461

462 **JAK2V617F EC Drive Neoplastic Angiogenesis and Dysregulate Cellular**
463 **Crosstalk in 3D Complex Cocultures**

464 In cocultures with JAK2V617F restricted to iEC (HET-WT), the endothelium
465 exhibited a pro-mesenchymal phenotype, characterized by elevated expression of
466 EndMT markers, including *ACTA2*, *FSP1* (*S100A4*), and *FAP*, as confirmed by RNA-
467 seq (Fig. 8D, Supplementary Fig. 9A). Consistent with the hyperproliferative phenotype
468 of mutated iEC (Fig. 1B), 3D cocultures with JAK2V617F^{HET} iEC exhibited a significant
469 increase in relative EC numbers compared to WT controls, an effect further amplified
470 in the presence of JAK2V617F^{HET} iHC (Supplementary Fig. 9B). In the presence of

471 mutated iHC, JAK2V617F^{HET} iEC displayed additional upregulation of the mid-stage
472 EndMT marker *DEPP1*[44], alongside *ACTA2* and *SNAI1*, as well as increased
473 expression of glycolysis-related genes such as *MYC*, *LDH*, and *GAPDH* (Fig. 8D,
474 Supplementary Fig. 9C), indicating advanced EndMT.

475 To investigate the impact of JAK2V617F EC on cellular crosstalk, we analyzed
476 L-R interactions within HET-WT cocultures (Supplementary Fig. 9D). JAK2V617F^{HET}
477 iEC exhibited reduced interactions with other niche components, particularly through
478 the key vascular basement membrane protein COL4A1/2 and calmodulin-1 (CALM1),
479 a protein essential for eNOS activity, whose downregulation has been associated with
480 endothelial cell impairment[45]. Despite an overall reduction in crosstalk strength,
481 basophil progenitors showed enhanced signaling via FN1 (ITGAV/CD44) and
482 intensified interactions with neutrophils, mast cells, and stromal cells through the
483 SPP1-CD44 axis. Elevated SPP1, CD44, and FN1 levels are linked to poor cancer
484 prognosis due to their involvement in remodeling the tumor microenvironment[46,47].
485 These dysregulations in HET-WT cocultures underscore the mutant vascular niche's
486 role in BM remodeling and potential contribution to cardiovascular complications in
487 JAK2V617F+ MPN patients.

488

489 **IFNα inhibits EndMT progression in JAK2V617F 3D Complex Cocultures**

490 To evaluate the effects of IFNα on the neoplastic vasculature and BM niche,
491 JAK2V617F 3D complex cocultures were treated with IFNα (1000 U/mL) for 48 hours
492 prior to scRNAseq (Fig. 7A). Again, crosstalk analysis identified basophil progenitors
493 as a key signaling hub, displaying strong interactions with various cell types, including
494 stromal cells, pericytes, mast cells, and EC through ECM components (e.g., collagen,
495 FN1, SPP1) and growth factors (e.g., CXCL, VEGF) (Fig. 9A-B). Treatment with IFNα
496 robustly activated the IFNα downstream JAK-STAT pathway in most hematopoietic

497 lineages. This response was less pronounced in CD45- lineages, where only MSC
498 clusters 1 and 5 and iEC showed similar JAK-STAT activation. Correspondingly,
499 reactome pathway analysis revealed varied upregulation of IFNα signaling genes
500 across different hematopoietic and stromal subsets (Fig. 9C). Consistent with our
501 previous findings, IFNα treatment demonstrated anti-EndMT properties, significantly
502 downregulating key EndMT markers *ACTA2*, *COL1A1*, and Vimentin (*VIM*) in mutated
503 iEC (Fig. 8D). Additionally, IFNα reversed the hyperproliferative phenotype of
504 JAK2V617F^{HET} iEC (Supplementary Fig. 9B), and decreased interactions strength
505 mediated via laminin and angiogenic factors (e.g., VEGF, MK, ANGPTL) (Fig. 9D).
506 Furthermore, IFNα partially diminished the previously observed pro-inflammatory
507 profile of JAK2V617F^{HET} cocultures, including the downregulation of hypoxia-related
508 pathways in neutrophils (clusters 17 and 8), monocytes (clusters 0 and 3), dendritic
509 cells (cluster 12), mast cells (clusters 2 and 7), hemogenic endothelium (cluster 16),
510 EC (cluster 13), and various MSC subsets (clusters 1, 5, 6, 11) (Fig. 9C).
511 Thus, in addition to its previously described anti-angiogenic properties, our
512 scRNA-seq results highlight cell type-specific transcriptional changes following IFNα
513 treatment, suggesting niche-specific alterations with significant implications for the
514 malignant clone microenvironment.
515

516 **Discussion**

517 Advances in stem cell biology enable iPSC differentiation into specific cell types,
518 providing patient-specific models for disease research and drug screening[48,49]. To
519 study the pro-fibrotic role of the JAK2V617F-bearing vascular niche, we employed
520 patient-derived JAK2V617F$^{HET\ and\ HOM}$ iEC. While JAK2V617F zygosity did not impact
521 endothelial differentiation, JAK2V617F iEC showed a hyperproliferative phenotype,
522 reflecting the abnormal neoangiogenesis seen in MPN patient spleen and BM[3,4].

523 Treatment of iEC with compounds used or under study for MPN revealed distinct
524 vascular toxicity profiles, matching clinical features such as potential vascular side
525 effects of anagrelide[50] and venetoclax[51], while ruxolitinib, AMG-232, hydroxyurea, and
526 IFNα showed more favorable profiles. IFNα, approved for polycythemia vera (PV)
527 therapy, has shown in long-term studies to increase myelofibrosis-free survival and
528 achieve near-normal life expectancy, unlike hydroxyurea- or phlebotomy only-treated
529 PV patients[13,52]. However, its therapeutic mechanisms and impact on the malignant
530 BM microenvironment remain unclear.

531 To address the limitations of 2D culture, we developed a 3D MSC-iEC coculture
532 model that effectively replicates the critical heterotypic interactions between pericytes,
533 and EC required during vasculogenesis. Previous *in vivo* studies showed that acute
534 IFNα exposure increased BM vascularity[53], while chronic exposure inhibited
535 angiogenesis by inducing EC senescence and reducing the secretion of proangiogenic
536 factors like VEGF[15,54]. Our 3D model results align with these findings: acute IFNα
537 exposure promoted a trend toward increased vascular network formation, while
538 repeated exposure, with separate pre-treatment of iEC and MSC, significantly impaired
539 vasculogenesis.

540 Recent studies have highlighted the impact of JAK2V617F-zygosity on MPN
541 disease severity and associated complications[55]. Consistent with these findings, our
542 global RNA-seq analysis revealed distinct zygosity-dependent transcriptional
543 signatures in iEC under both basal conditions and following IFNα treatment. These
544 results align with reports showing heightened activation of pathways such as AKT,
545 STAT5, and ERK1/2 in JAK2V617F erythroblasts, with signaling further intensified in
546 JAK2V617F$^{HOM\ vs.\ HET}$ erythroblasts[56], providing a mechanistic basis for the zygosity-
547 dependent gene expression differences observed in our study.

548 In line with recent work linking JAK2V617F EC to EndMT and MPN-associated
549 cardiovascular dysfunction[57], we found that JAK2V617F^{HET} iEC exhibited a pro-
550 mesenchymal phenotype, characterized by the upregulation of key EndMT markers
551 such as *FSP1* and *ACTA2*. AKT and ERK1/2 dysregulated signaling in JAK2V617F
552 EC may drive the observed phenotype and contribute to ECM remodeling[24]. In
553 contrast, JAK2V617F^{HOM} iEC exhibited substantial transcriptional downregulation of
554 protein translation machinery and disrupted ribosome-ER organization, as observed
555 by TEM. This effect may be driven by AKT-mediated ROS accumulation, a feature of
556 JAK2V617F^{HOM} signaling[58], which in turn disrupts translation and impairs ribosome
557 biogenesis[59]. However, it should not be excluded that JAK2V617F^{HOM} iEC's
558 hyperproliferation affects ribosomal subcellular organization.
559 IFNα treatment of JAK2V617F^{HOM} iEC upregulated ribosome biogenesis and RNA
560 splicing pathways, suggesting a restoration of dysregulated translation machinery
561 observed under basal conditions. Importantly, this effect was not linked to apoptosis,
562 consistent with IFNα's favorable vascular toxicity profile. These findings highlight
563 IFNα's potential to address zygosity-driven phenotypic alterations in JAK2V617F iEC.
564 Increasing evidence highlights the functional link between inflammation,
565 thrombosis, and the role of EndMT in tissue remodeling[5,60]. In our 3D iEC-MSC
566 cocultures, TGFβ, IL1β, and TNFα effectively induced EndMT, emphasizing
567 JAK2V617F^{HET} iEC's pro-mesenchymal phenotype. While IFNα partially inhibited this
568 cytokine-driven EndMT phenotype *in vitro*, it significantly blocked EndMT *in vivo*. The
569 stronger anti-EndMT effect of IFNα *in vivo* may result from the chronic treatment
570 regimens used in mice and MPN patients, contrasting with the short incubation period
571 in our 3D model. This aligns with clinical observations that IFNα acts as a rather slow-
572 acting drug[61].

573 Building on the prevalence of JAK2V617F heterozygosity in MPN patients[62], we
574 then investigated how the mutant endothelium influences the BM niche across diverse
575 hematopoietic genetic backgrounds. scRNA-seq analysis of 3D complex cocultures
576 identified key myeloid and non-hematopoietic lineages, including EC and various MSC
577 clusters, mirroring the stromal heterogeneity of the human BM niche[38]. Despite the
578 JAK2V617F driver mutation being commonly shared by hematopoietic cells and EC[63],
579 we generated cocultures exclusively harboring JAK2V617F^{HET} in EC to individually
580 dissect the properties of the mutant endothelium and its impact on niche remodeling.
581 Consistent with our previous findings, JAK2V617F^{HET} iEC displayed a mesenchymal
582 phenotype. Notably, cocultures with mutated iEC exhibited a reduction in predicted L-
583 R interaction strength compared to unmutated cocultures, aligning with previous
584 research evidencing that the JAK2V617F-bearing vascular niche preferentially
585 supports JAK2V617F clonal expansion[7]. Interestingly, basophil progenitors showed
586 increased interactions with niche components via FN1, a potential biomarker for early
587 myelofibrotic transformation[64]. L-R analysis also revealed enhanced crosstalk between
588 basophil progenitors and MSC through SPP1, a glycoprotein known to promote a
589 fibrotic microenvironment[65]. Aligning with previous work[66], these enhanced interactions
590 suggest that specific cell types and pro-inflammatory pathways become hyperactive in
591 response to JAK2V617F EC, driving microenvironmental remodeling and vascular
592 complications, even in the absence of JAK2V617F hematopoietic cells.

593 In the presence of JAK2V617F^{HET} iHC, EC dysfunction was exacerbated,
594 marked by upregulated EndMT markers, and heightened glycolytic activity, suggesting
595 progression toward advanced EndMT[67]. Moreover, JAK2V617F^{HET} cocultures
596 recapitulated hallmark MPN features, such as upregulated hypoxic[26] and TGFβ
597 signaling[40] in critical fibrosis-associated cell types, including monocytes,
598 macrophages, neutrophils, MSC, and mast cells[36,38]. Partial TNFα downregulation in

599 specific stromal and hematopoietic subsets hints at a possible mechanism for limiting
600 inflammation and sustaining MSC immunosuppressive properties, as previously
601 described[68]. In JAK2V617F^{HET} cocultures, monocytes, neutrophils, and mast cells
602 exhibited increased IFNα signaling, in line with earlier findings of interferon-stimulated
603 genes upregulation in JAK2V617F hematopoietic cells[69]. Mapping of L-R pairs further
604 highlighted basophil progenitors and stromal cells (MSC, EC, and pericytes) as key
605 orchestrators in both unmutated and mutated niches. Increased interactions among
606 these cell types and other niche components via central fibrotic pathways, such as
607 MIF-CD74[42] and LGALS1-ITGB1[43], underscore their pivotal role in driving BM niche
608 fibrosis, positioning them as promising therapeutic targets in MPN.

609 scRNA-seq analysis of 3D cocultures treated with IFNα revealed that IFNα
610 effectively suppressed JAK2V617F iEC hyperproliferation and partially reversed their
611 EndMT phenotype. Notably, the upregulation of genes linked to TGFβ signaling in EC
612 suggests vascular normalization, as TGFβ has been shown to enhance endothelial
613 barrier function and plays a vital role in vasculogenesis[70]. IFNα treatment mitigated the
614 pro-inflammatory and pro-fibrotic profile observed in JAK2V617F^{HET} 3D complex
615 cocultures, while selectively upregulating the expression of IFNα signaling-related
616 genes across both hematopoietic and stromal subsets. These findings are particularly
617 relevant considering recent evidence showing a tonic autocrine IFNα loop in EC[15] and
618 JAK1/STAT1-mediated sensitization to IFNα in JAK2V617F+ patients[69].

619 Our scalable fibrin-based 3D coculture system offers an accessible,
620 reproducible platform for mechanistic studies with precise control over cellular
621 composition and genetic background, yet it has limitations. It does not fully capture the
622 BM niche's complexity in terms of cellularity and spatial architecture. The currently
623 short cultivation period may not align with the slow-developing nature of fibrosis,
624 potentially limiting its predictive value to early-stage fibrosis. Incorporating additional

625 niche components (e.g., lymphoid and neuronal cells), optimizing matrix composition,
626 and introducing flow conditions could extend cultivation time and enhance its
627 translational relevance. Despite its limitations, our 3D iPSC-based model captures
628 essential features of normal and neoplastic hematopoiesis described in human and
629 murine studies, underscoring its utility for mechanistic studies of the BM niche.

630 This study uncovers JAK2V617F zygosity-associated phenotypic variability in
631 EC, suggesting mutational burden as a key driver of vascular dysfunction and BM
632 fibrosis in MPN. Further single-cell and spatial transcriptomics studies are warranted
633 to dissect the JAK2V617F mutational burden in the vascular tissue of MPN patients
634 and facilitate the clinical translation of our findings. Moreover, we present the first
635 evidence, to our knowledge, that IFNα inhibits EndMT, unveiling a previously
636 unrecognized mechanism for its anti-fibrotic and anti-angiogenic effects. These
637 findings pave the way for innovative strategies to target the vascular
638 microenvironment, offering new opportunities to mitigate MF and improve patient
639 outcomes.

640

641 **Acknowledgements**

642 This study was supported by the Confocal Microscopy Facility (MCF), the Flow
643 Cytometry Facility (FCF), the Genomics Facility (GF), the Two Photon Imaging Facility
644 (2PIF), and the Immunohistochemistry Facility (IHF), all Core Facilities of the
645 Interdisciplinary Center for Clinical Research (IZKF) Aachen within the Faculty of
646 Medicine at RWTH Aachen University. Transmission Electron Microscopy was
647 performed in the Institute of Pathology and Electron Microscopy Facility, RWTH
648 Aachen. Finally, we would like to thank all the patients who kindly donated samples.

649

This study was in part funded by grants to Marcelo A. S. de Toledo from the RWTH Aachen University START grant (128/22), to Steffen Koschmieder from the German Research Foundation (Deutsche Forschungsgemeinschaft, DFG) (KO 2155/6-1) and by funds from German Research Foundation as part of the Clinical Research Unit CRU 344 to SK, NC, IC and THB (KO2155/7-1, CH1509/1-1, GE2811/4-1 and BR1782/5-1). Madeline J. Caduc was funded by the Clinician Scientist Program Junior and the "FF-Med" funding program for female doctors in the post-doc phase of the Faculty of Medicine, RWTH Aachen, Germany.

Author Contributions

M. J. C.: conceptualization, formal analysis, investigation, visualization, methodology, manuscript–original draft, writing–review and editing. **M. H. E. M.:** methodology. **C. B. L.:** methodology. **M. G.:** methodology. **E. M. B.:** methodology, visualization. **S. E.:** methodology, visualization. **D. W. L. W.:** methodology, visualization. **G. M-N.:** resources, investigation, writing-review, and editing. **M. V.:** methodology, visualization. **J. E.:** resources. **P. B.:** resources, investigation, methodology. **M. A.:** resources, investigation, methodology. **N. C.:** resources, writing-review, and editing. **J. F.:** methodology, writing-review, and editing. **I. G. C.:** resources, methodology. **M. Z.:** resources, investigation, writing-review, and editing. **R. K. S.:** resources, writing-review, and editing**. T. H. B.:** resources, funding acquisition, writing-review, and editing. **S. K.:** conceptualization, supervision, resources, funding acquisition, project administration, investigation, data analysis, writing-review, and editing. **M. A. S. T.:** conceptualization, supervision, resources, funding acquisition, project administration, investigation, methodology, formal analysis, writing-review, and editing.

677 **Conflict-of-interest disclosure**

678 **S. K.** received research grant/funding from Geron, Janssen, AOP Pharma, and
679 Novartis; received consulting fees from Pfizer, Incyte, Ariad, Novartis, AOP Pharma,
680 Bristol Myers Squibb, Celgene, Geron, Janssen, CTI BioPharma, Roche, Bayer, GSK,
681 Protagonist, MSD, mPN Hub, Bedrock, and PharmaEssentia; received payment or
682 honoraria from Novartis,BMS/Celgene, Pfizer, Incyte, AOP Orphan, GSK, AbbVie,
683 MSD, MPN Hub, Bedrock, iOMEDICO; received travel/accommodation support from
684 Alexion, Novartis, Bristol Myers Squibb, Incyte, AOP Pharma, CTI BioPharma, Pfizer,
685 Celgene, Janssen, Geron, Roche, AbbVie, GSK, Sierra Oncology, Kartos, Imago
686 Biosciences, MSD, and iOMEDICO; had a patent issued for a BET inhibitor at RWTH
687 Aachen University; participated on advisory boards for Pfizer, Incyte, Ariad, Novartis,
688 AOP Pharma, BMS, Celgene, Geron, Janssen, CTI BioPharma, Roche, Bayer, GSK,
689 Sierra Oncology, AbbVie, Protagonist, MSD, and PharmaEssentia. **T. H. B.** served as
690 consultant/speaker for Gilead, Janssen, Merck, Novartis, Pfizer, and received research
691 support from Novartis and Pfizer.

692

693 **References**

694 1. Vannucchi, A. M. *et al.* Mutations and prognosis in primary myelofibrosis. *Leukemia*
695 **27**, 1861–1869 (2013).
696 2. Barbui, T. *et al.* Thrombosis in primary myelofibrosis: incidence and risk factors.
697 *Blood* **115**, 778–782 (2010).
698 3. Boveri, E. *et al.* Bone marrow microvessel density in chronic myeloproliferative
699 disorders: a study of 115 patients with clinicopathological and molecular correlations. *Br J*
700 *Haematol* **140**, 162–168 (2008).
701 4. Barosi, G. *et al.* Spleen neoangiogenesis in patients with myelofibrosis with myeloid
702 metaplasia. *British Journal of Haematology* **124**, 618–625 (2004).
703 5. Erba, B. G. *et al.* Endothelial-to-Mesenchymal Transition in Bone Marrow and Spleen
704 of Primary Myelofibrosis. *The American Journal of Pathology* **187**, 1879–1892 (2017).
705 6. Ding, L., Saunders, T. L., Enikolopov, G. & Morrison, S. J. Endothelial and
706 perivascular cells maintain haematopoietic stem cells. *Nature* **481**, 457–462 (2012).
707 7. Zhan, H., Lin, C. H. S., Segal, Y. & Kaushansky, K. The JAK2V617F-bearing
708 vascular niche promotes clonal expansion in myeloproliferative neoplasms. *Leukemia* **32**,
709 462–469 (2018).
710 8. Sozer, S. *et al.* The presence of JAK2V617F mutation in the liver endothelial cells of
711 patients with Budd-Chiari syndrome. *Blood* **113**, 5246–5249 (2009).

712 9. Rosti, V. *et al.* Spleen endothelial cells from patients with myelofibrosis harbor the
713 JAK2V617F mutation. *Blood* **121**, 360–368 (2013).
714 10. Dzierzak, E. & Bigas, A. Blood Development: Hematopoietic Stem Cell Dependence
715 and Independence. *Cell Stem Cell* **22**, 639–651 (2018).
716 11. Eilken, H. M., Nishikawa, S.-I. & Schroeder, T. Continuous single-cell imaging of
717 blood generation from haemogenic endothelium. *Nature* **457**, 896–900 (2009).
718 12. Bewersdorf, J. P. *et al.* Moving toward disease modification in polycythemia vera.
719 *Blood* **142**, 1859–1870 (2023).
720 13. Abu-Zeinah, G. *et al.* Interferon-alpha for treating polycythemia vera yields improved
721 myelofibrosis-free and overall survival. *Leukemia* **35**, 2592–2601 (2021).
722 14. Indraccolo, S. Interferon-α as angiogenesis inhibitor: Learning from tumor models.
723 *Autoimmunity* **43**, 244–247 (2010).
724 15. Ciccarese, F. *et al.* Genetic perturbation of IFN-α transcriptional modulators in human
725 endothelial cells uncovers pivotal regulators of angiogenesis. *Comput Struct Biotechnol J* **18**,
726 3977–3986 (2020).
727 16. Shi, Y., Inoue, H., Wu, J. C. & Yamanaka, S. Induced pluripotent stem cell
728 technology: a decade of progress. *Nat Rev Drug Discov* **16**, 115–130 (2017).
729 17. Méndez-Ferrer, S. *et al.* Mesenchymal and haematopoietic stem cells form a unique
730 bone marrow niche. *Nature* **466**, 829–834 (2010).
731 18. Sweeney, M. & Foldes, G. It Takes Two: Endothelial-Perivascular Cell Cross-Talk in
732 Vascular Development and Disease. *Frontiers in Cardiovascular Medicine* **5**, (2018).
733 19. Flosdorf, N. *et al.* Proinflammatory phenotype of iPS cell-derived JAK2 V617F
734 megakaryocytes induces fibrosis in 3D in vitro bone marrow niche. *Stem Cell Reports* **19**,
735 224–238 (2024).
736 20. Olschok, K. *et al. Stem Cell Reports* **16**, 2768–2783 (2021).
737 21. Strassburg, S. *et al.* In vivo evaluation of an electrospun gelatin nonwoven mat for
738 regeneration of epithelial tissues. *Journal of Biomedical Materials Research Part A* **107**,
739 1605–1614 (2019).
740 22. Nassiri, S. M. & Rahbarghazi, R. Interactions of Mesenchymal Stem Cells with
741 Endothelial Cells. *Stem Cells and Development* **23**, 319–332 (2014).
742 23. Paik, D. T. *et al.* Large-Scale Single-Cell RNA-Seq Reveals Molecular Signatures of
743 Heterogeneous Populations of Human Induced Pluripotent Stem Cell-Derived Endothelial
744 Cells. *Circ Res* **123**, 443–450 (2018).
745 24. Piera-Velazquez, S. & Jimenez, S. A. Endothelial to Mesenchymal Transition: Role in
746 Physiology and in the Pathogenesis of Human Diseases. *Physiol Rev* **99**, 1281–1324 (2019).
747 25. Bjørn, M. E. & Hasselbalch, H. C. The Role of Reactive Oxygen Species in
748 Myelofibrosis and Related Neoplasms. *Mediators Inflamm* **2015**, 648090 (2015).
749 26. Baumeister, J. *et al.* Hypoxia-inducible factor 1 (HIF-1) is a new therapeutic target in
750 JAK2V617F-positive myeloproliferative neoplasms. *Leukemia* **34**, 1062–1074 (2020).
751 27. Gilles, L. *et al.* Downregulation of GATA1 drives impaired hematopoiesis in primary
752 myelofibrosis. *J Clin Invest* **127**, 1316–1320.
753 28. Gulìa, C. *et al.* Y RNA: An Overview of Their Role as Potential Biomarkers and
754 Molecular Targets in Human Cancers. *Cancers (Basel)* **12**, 1238 (2020).
755 29. Han, C. *et al.* Chromatin-associated orphan snoRNA regulates DNA damage-mediated
756 differentiation via a non-canonical complex. *Cell Rep* **38**, 110421 (2022).
757 30. Patel, A. A. & Steitz, J. A. Splicing double: insights from the second spliceosome. *Nat*
758 *Rev Mol Cell Biol* **4**, 960–970 (2003).
759 31. Wang, S. *et al.* RNU12 inhibits gastric cancer progression via sponging miR-575 and
760 targeting BLID. *Sci Rep* **13**, 7523 (2023).
761 32. Liu, Z. *et al.* SNORA23 inhibits HCC tumorigenesis by impairing the 2′-O-ribose
762 methylation level of 28S rRNA. *Cancer Biol Med* **19**, 104–119 (2022).

33. Kvasnicka, H. M. *et al.* Long-term effects of ruxolitinib versus best available therapy on bone marrow fibrosis in patients with myelofibrosis. *J Hematol Oncol* **11**, 42 (2018).
34. Bai, Y. *et al.* Ruxolitinib Alleviates Renal Interstitial Fibrosis in UUO Mice. *International Journal of Biological Sciences* **16**, 194–203 (2020).
35. Yu, W.-K. *et al.* Nintedanib Inhibits Endothelial Mesenchymal Transition in Bleomycin-Induced Pulmonary Fibrosis via Focal Adhesion Kinase Activity Reduction. *Int J Mol Sci* **23**, 8193 (2022).
36. Toledo, M. A. S., Chatain, N., Zenke, M. & Koschmieder, S. Mast cells as a therapeutic target in myeloproliferative neoplasms. *Trends in Molecular Medicine* **28**, 902–905 (2022).
37. Schneider, R. K. *et al.* Gli1+ Mesenchymal Stromal Cells Are a Key Driver of Bone Marrow Fibrosis and an Important Cellular Therapeutic Target. *Cell Stem Cell* **20**, 785-800.e8 (2017).
38. Leimkühler, N. B. *et al.* Heterogeneous bone-marrow stromal progenitors drive myelofibrosis via a druggable alarmin axis. *Cell Stem Cell* **28**, 637-652.e8 (2021).
39. Huang, E. *et al.* The Roles of Immune Cells in the Pathogenesis of Fibrosis. *International Journal of Molecular Sciences* **21**, 5203 (2020).
40. Meng, X.-M., Nikolic-Paterson, D. J. & Lan, H. Y. TGF-β: the master regulator of fibrosis. *Nat Rev Nephrol* **12**, 325–338 (2016).
41. Sarkaria, S. M. *et al.* Systematic dissection of coordinated stromal remodeling identifies *Sox10*+ glial cells as a therapeutic target in myelofibrosis. *Cell Stem Cell* **30**, 832-850.e6 (2023).
42. Pritchard, J. E. *et al.* Non-canonical Hedgehog signaling mediates profibrotic hematopoiesis-stroma crosstalk in myeloproliferative neoplasms. *Cell Rep* **43**, 113608 (2024).
43. Li, R. *et al.* A proinflammatory stem cell niche drives myelofibrosis through a targetable galectin-1 axis. *Sci Transl Med* **16**, eadj7552 (2024).
44. Slenders, L. *et al.* Identification of endothelial-to-mesenchymal transition gene signatures in single-cell transcriptomics of human atherosclerotic tissue. 2023.07.18.549599 Preprint at https://doi.org/10.1101/2023.07.18.549599 (2023).
45. Liu, T. *et al.* Downregulated calmodulin expression contributes to endothelial cell impairment in diabetes. *Acta Pharmacol Sin* **44**, 2492–2503 (2023).
46. Xie, W. *et al.* Multi-Transcriptomic Analysis Reveals the Heterogeneity and Tumor-Promoting Role of SPP1/CD44-Mediated Intratumoral Crosstalk in Gastric Cancer. *Cancers* **15**, 164 (2022).
47. Wang, H. *et al.* FN1 is a prognostic biomarker and correlated with immune infiltrates in gastric cancers. *Frontiers in Oncology* **12**, 918719 (2022).
48. Khan, A. O. *et al.* Human Bone Marrow Organoids for Disease Modeling, Discovery, and Validation of Therapeutic Targets in Hematologic Malignancies. *Cancer Discovery* **13**, 364 (2023).
49. Frenz-Wiessner, S. *et al.* Generation of complex bone marrow organoids from human induced pluripotent stem cells. *Nat Methods* (2024) doi:10.1038/s41592-024-02172-2.
50. James, C. W. Anagrelide-induced cardiomyopathy. *Pharmacotherapy* **20**, 1224–1227 (2000).
51. AlAsmari, A. F. *et al.* Venetoclax Induces Cardiotoxicity through Modulation of Oxidative-Stress-Mediated Cardiac Inflammation and Apoptosis via NF-κB and BCL-2 Pathway. *Int J Mol Sci* **23**, 6260 (2022).
52. Abu-Zeinah, G., Silver, R. T., Abu-Zeinah, K. & Scandura, J. M. Normal life expectancy for polycythemia vera (PV) patients is possible. *Leukemia* **36**, 569–572 (2022).
53. Prendergast, Á. M. *et al.* IFNα-mediated remodeling of endothelial cells in the bone marrow niche. *Haematologica* **102**, 445–453 (2017).
54. Pammer, J. *et al.* Interferon-a prevents apoptosis of endothelial cells after short-term

exposure but induces replicative senescence after continuous stimulation. *Laboratory Investigation* 11 (2006).
55. Moliterno, A. R., Kaizer, H. & Reeves, B. N. JAK2 V617F allele burden in polycythemia vera: burden of proof. *Blood* **141**, 1934–1942 (2023).
56. Akada, H. *et al.* Conditional expression of heterozygous or homozygous Jak2V617F from its endogenous promoter induces a polycythemia vera-like disease. *Blood* **115**, 3589–3597 (2010).
57. Zhang, H. *et al.* Decoding Endothelial MPL and JAK2V617F Mutation: Insight Into Cardiovascular Dysfunction in Myeloproliferative Neoplasms. *Arterioscler Thromb Vasc Biol* **44**, 1960–1974 (2024).
58. Marty, C. *et al.* A role for reactive oxygen species in JAK2 V617F myeloproliferative neoplasm progression. *Leukemia* **27**, 2187–2195 (2013).
59. Willi, J. *et al.* Oxidative stress damages rRNA inside the ribosome and differentially affects the catalytic center. *Nucleic Acids Research* **46**, 1945–1957 (2018).
60. Alvandi, Z. & Bischoff, J. Endothelial-Mesenchymal Transition in Cardiovascular Disease. *Arterioscler Thromb Vasc Biol* **41**, 2357–2369 (2021).
61. Gisslinger, H. *et al.* Long-Term Efficacy and Safety of Ropeginterferon Alfa-2b in Patients with Polycythemia Vera — Final Phase I/II Peginvera Study Results. *Blood* **132**, 3030 (2018).
62. Tefferi, A. & Vainchenker, W. Myeloproliferative Neoplasms: Molecular Pathophysiology, Essential Clinical Understanding, and Treatment Strategies. *Journal of Clinical Oncology* (2011) doi:10.1200/JCO.2010.29.8711.
63. Farina, M. *et al.* Comparative Mutational Profiling of Hematopoietic Progenitor Cells and Circulating Endothelial Cells (CECs) in Patients with Primary Myelofibrosis. *Cells* **10**, 2764 (2021).
64. Schneider, R. K. *et al.* Activated fibronectin-secretory phenotype of mesenchymal stromal cells in pre-fibrotic myeloproliferative neoplasms. *J Hematol Oncol* **7**, 92 (2014).
65. Ruberti, S. *et al.* Involvement of MAF/SPP1 axis in the development of bone marrow fibrosis in PMF patients. *Leukemia* **32**, 438–449 (2018).
66. Guy, A. *et al.* Vascular endothelial cell expression of JAK2 ^{V617F} is sufficient to promote a pro-thrombotic state due to increased P-selectin expression. *Haematologica* **104**, 70–81 (2019).
67. Xiong, J. *et al.* A Metabolic Basis for Endothelial-to-Mesenchymal Transition. *Molecular Cell* **69**, 689-698.e7 (2018).
68. Li, W., Liu, Q., Shi, J., Xu, X. & Xu, J. The role of TNF-α in the fate regulation and functional reprogramming of mesenchymal stem cells in an inflammatory microenvironment. *Front. Immunol.* **14**, (2023).
69. Czech, J. *et al.* JAK2V617F but not CALR mutations confer increased molecular responses to interferon-α via JAK1/STAT1 activation. *Leukemia* **33**, 995–1010 (2019).
70. Armulik, A., Abramsson, A. & Betsholtz, C. Endothelial/Pericyte Interactions. *Circulation Research* **97**, 512–523 (2005).

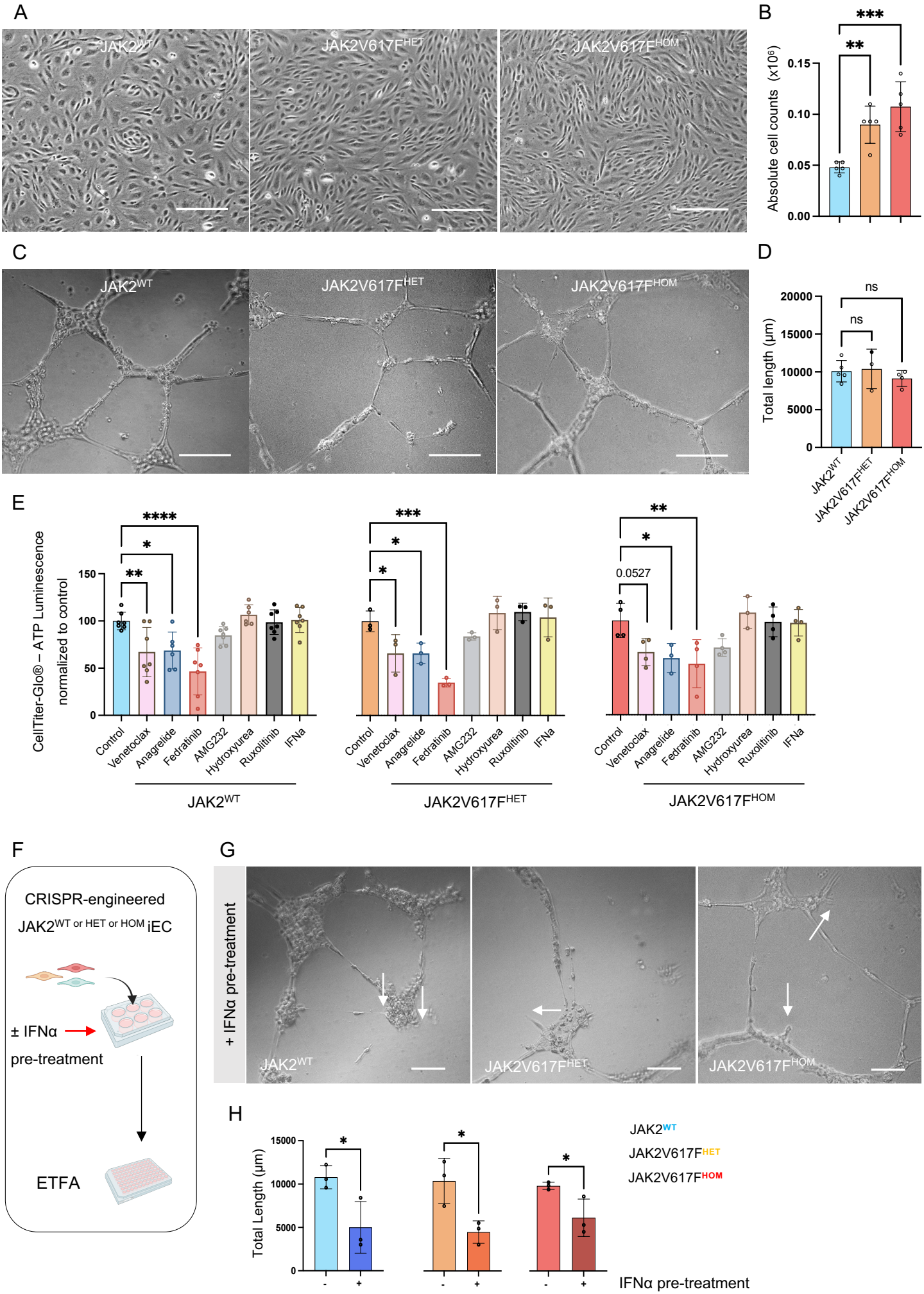
A
JAK2WT
JAK2V617FHET
JAK2V617FHOM
B
Absolute cell counts (x10^6)
0.15
0.10
0.05
0.00
**
***
C
JAK2WT
JAK2V617FHET
JAK2V617FHOM
D
Total length (µm)
20000
15000
10000
5000
0
ns
ns
JAK2WT
JAK2V617FHET
JAK2V617FHOM
E
CellTiter-Glo® – ATP Luminescence normalized to control
150
100
50
0
****
***
**
*
0.0527
Control
Venetoclax
Anagrelide
Fedratinib
AMG232
Hydroxyurea
Ruxolitinib
IFNa
JAK2WT
JAK2V617FHET
JAK2V617FHOM
F
CRISPR-engineered
JAK2WT or HET or HOM iEC
± IFNα
pre-treatment
ETFA
G
+ IFNα pre-treatment
JAK2WT
JAK2V617FHET
JAK2V617FHOM
H
Total Length (µm)
15000
10000
5000
0
*
-
+
JAK2WT
JAK2V617FHET
JAK2V617FHOM
IFNα pre-treatment

863 **Figure 1**. **MPN patient specific iPSC-derived EC to investigate IFNα's impact on**
864 **the vascular niche**

865 (A) Representative images of JAK2^{WT}, JAK2V617F^{HET}, and JAK2V617F^{HOM} iEC.
866 Scale bars, 500 μm.

867 (B) For proliferation assays, iEC were seeded at a density of 20,000 cells per well
868 in a 24-well plate, and cell counts were determined after 4 days of culture in
869 supplemented Endothelial Growth Medium-2 (EGM-2). One-way ANOVA (n =
870 5).

871 (C) To compare the angiogenic potential of mutated iEC to WT control, ETFA were
872 performed. Images were taken 12 to 14 hours after seeding the cells onto
873 Matrigel® or Geltrex® in a 96-well plate format. Scale bars, 200 μm.

874 (D) ETFA quantitative analysis comparing the total length of tubule-like structures
875 formed across three genotypes under basal conditions. One-way ANOVA (n =
876 3).

877 (E) To assess the response of iEC to clinically used or compounds under
878 investigation for MPN therapy, iEC were treated with 1 μM of the listed
879 compounds or 1000 U/ml IFNα. One-way ANOVA (n = 3-7).

880 (F) Experimental design used to explore the anti-angiogenic potential of IFNα.
881 ETFA were conducted with or without prior exposure of iEC to 1000 U/ml IFNα
882 before seeding onto reconstituted basement membrane.

883 (G) Photographs illustrating the effects of 1000 U/ml IFNα pre-sensitization on iEC.
884 White arrows highlight disrupted tubule-like structures. Scale bars, 100 μm.

885

886 (H) Quantitative analysis of ETFA comparing the total length of capillary-like
887 structures following iEC pre-treatment with 1000 U/ml IFNα. Unpaired t-test (n
888 = 3).

889
890

891

892

893

894

895

896

897

898

899

900

901

902

903

904

905

906

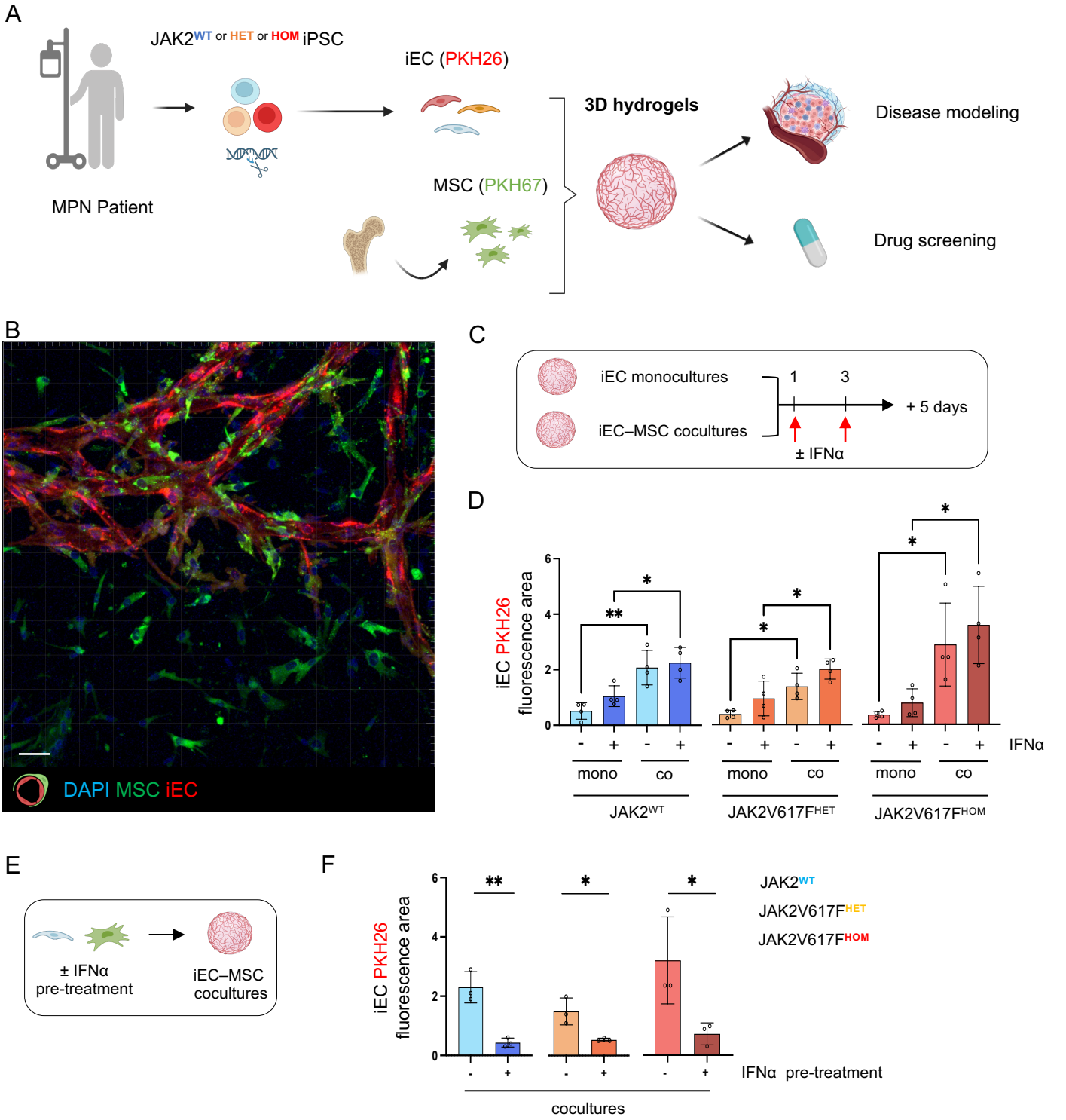
A
JAK2WT or HET or HOM iPSC
iEC (PKH26)
MPN Patient
MSC (PKH67)
3D hydrogels
Disease modeling
Drug screening
B
DAPI MSC iEC
C
iEC monocultures
iEC–MSC cocultures
1
3
+ 5 days
± IFNα
D
iEC PKH26 fluorescence area
IFNα
mono
co
JAK2WT
JAK2V617FHET
JAK2V617FHOM
E
± IFNα pre-treatment
iEC–MSC cocultures
F
iEC PKH26 fluorescence area
JAK2WT
JAK2V617FHET
JAK2V617FHOM
IFNα pre-treatment
cocultures

907 **Figure 2. Impact of IFNα on neoplastic vasculogenesis in a 3D iPSC-based**
908 **coculture model with MSC**

909 (A) Schematic illustration of the experimental design used to generate 3D
910 cocultures for investigating neoplastic vasculogenesis. CRISPR-engineered
911 MPN patient-derived iEC and primary MSC (MSC) isolated from healthy donors'
912 femoral heads were suspended within fibrin hydrogels, either as mono- or
913 cocultures. These 3D systems provide scalable platforms for disease modeling
914 and high-throughput *in vitro* drug screening.

915 (B) Fluorescent cell linkers PKH26 and PKH67 were used to label iEC (red) and
916 MSC (green), respectively, prior to suspension within fibrin hydrogels.
917 Representative confocal image illustrates MSC alignment along the walls of
918 formed tube-like structures, mirroring EC-pericyte arrangement. Nuclei are
919 stained with DAPI. Scale bar, 50 μm.

920 (C) Experimental layout used to investigate iEC-MSC crosstalk during
921 vasculogenesis and evaluate IFNα's effect on network formation. The 3D culture
922 medium was supplemented with 1000U/ml IFNα on days 1 and 3. After 5 days
923 of incubation, samples were fixed and analyzed by microscopy.

924 (D) Quantification of PKH26 fluorescence area to assess vascular network
925 formation in 3D iEC monocultures and iEC-MSC cocultures across different
926 genetic and treatment conditions. One-way ANOVA (n = 3-4).

927 (E) Experimental layout used to investigate the impact of IFNα pre-treatment on
928 vasculogenesis. Prior to 3D coculture, MSC and iEC were separately pre-
929 treated with IFNα (1000 U/ml).

930 (F) Quantitative analysis of PKH26 fluorescence comparing the impact of separate
931 iEC and MSC pre-treatment with 1000 U/ml IFNα prior to 3D cocultivation on
932 the total area of capillary-like structures. Unpaired t-test (n = 3).

933
934
935
936
937
938
939
940
941
942
943
944
945
946
947
948
949
950
951
952
953
954
955
956
957
958
959
960
961
962
963
964
965
966
967
968
969
970
971
972
973
974
975
976
977

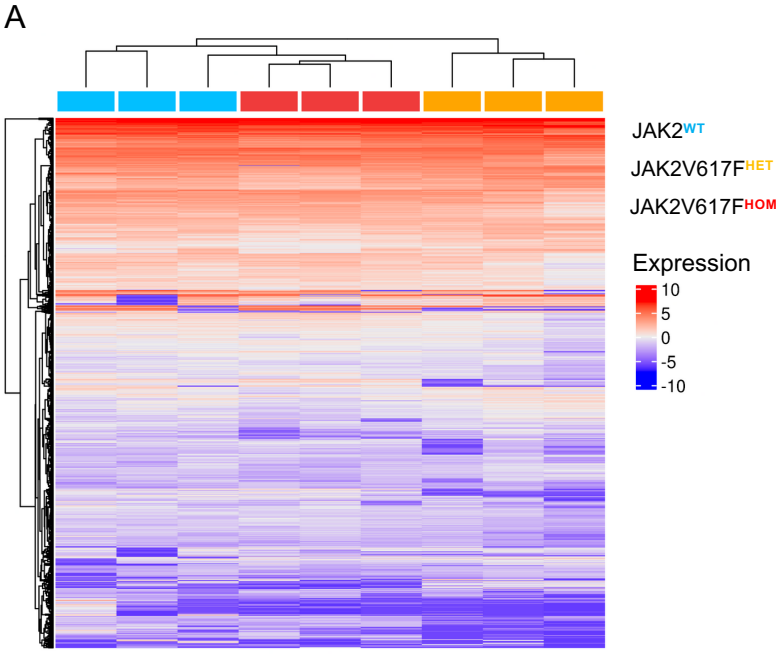
A
JAK2WT
JAK2V617FHET
JAK2V617FHOM
Expression
10
5
0
-5
-10

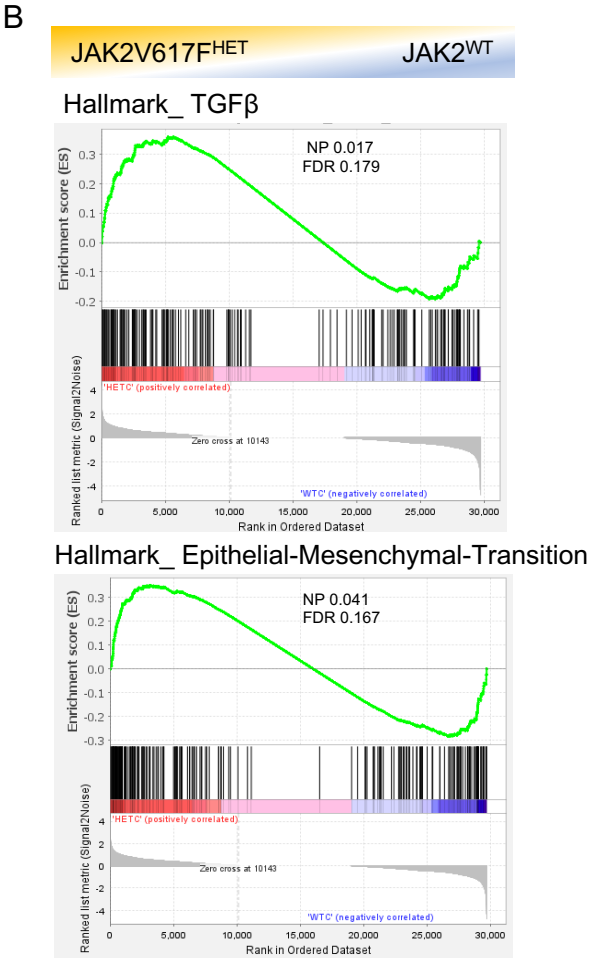
B
JAK2V617FHET
JAK2WT
Hallmark_ TGFβ
NP 0.017
FDR 0.179
Enrichment score (ES)
'HETC' (positively correlated)
Zero cross at 10143
'WTC' (negatively correlated)
Ranked list metric (Signal2Noise)
Rank in Ordered Dataset
Hallmark_ Epithelial-Mesenchymal-Transition
NP 0.041
FDR 0.167

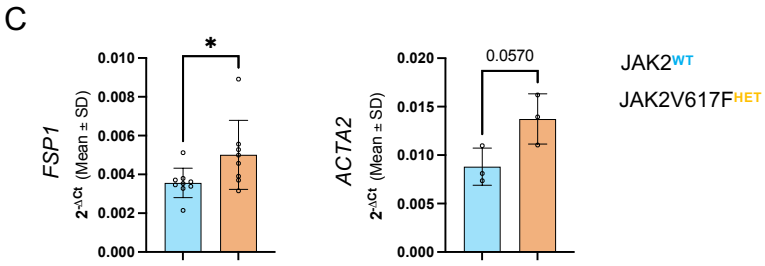
C
FSP1
ACTA2
2^-ΔCt (Mean ± SD)
*
0.0570
JAK2WT
JAK2V617FHET

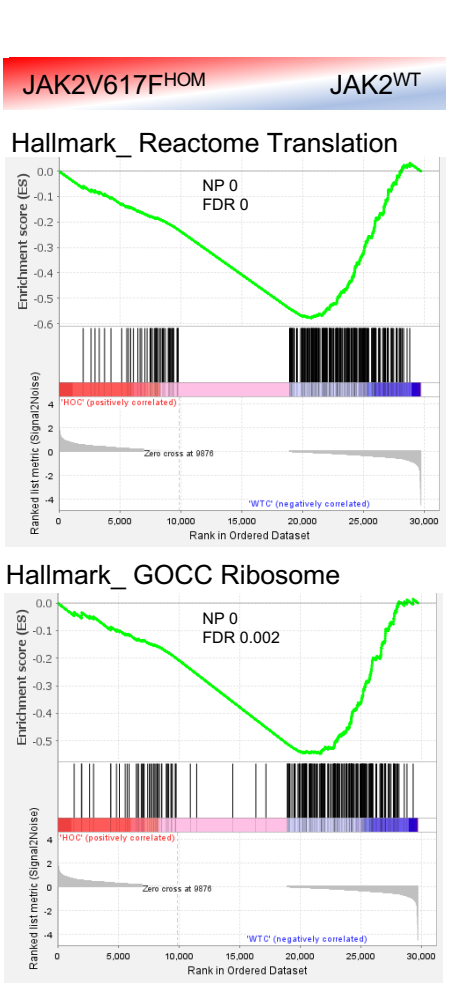
D
JAK2V617FHOM
JAK2WT
Hallmark_ Reactome Translation
NP 0
FDR 0
Enrichment score (ES)
'HOC' (positively correlated)
Zero cross at 9878
'WTC' (negatively correlated)
Ranked list metric (Signal2Noise)
Rank in Ordered Dataset
Hallmark_ GOCC Ribosome
NP 0
FDR 0.002

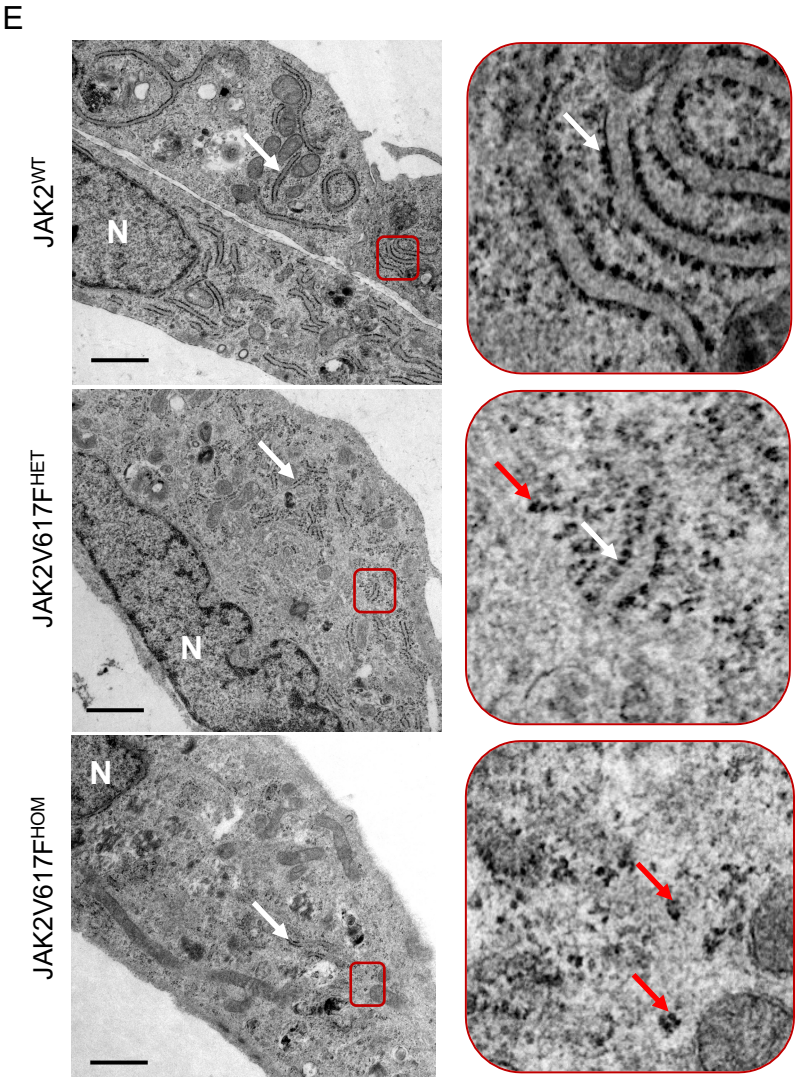
E
JAK2WT
JAK2V617FHET
JAK2V617FHOM
N

978 **Figure 3**. **Transcriptomic profiles of MPN patient-derived iEC**

979 (A) Heatmap depicting unsupervised clustering of differentially regulated genes in
980 JAK2^{WT} and JAK2V617F$^{HET\ and\ HOM}$ iEC (cut off: absolute logarithmic fold change
981 >1).

982 (B) Gene set enrichment analysis (GSEA) reveals the pro-mesenchymal and pro-
983 inflammatory transcriptional signature exhibited by JAK2V617F^{HET} iEC.
984 Abbreviations: NP, nominal p-value; FDR, false discovery rate.

985 (C) Quantification of mRNA levels of fibroblast-specific protein 1 (*FSP1*), alpha-
986 smooth muscle actin (*ACTA2*) by RT-qPCR in JAK2V617F^{HET} iEC, relative to
987 JAK2^{WT} iEC. Unpaired t-test (n = 3-8).

988 (D) Selection of dysregulated gene sets illustrating the prominent aspects detected
989 in the GSEA affecting JAK2V617F^{HOM} iEC biology. Abbreviations: NP, nominal
990 p-value; FDR, false discovery rate.

991 (E) Representative transmission electron microscopy images of iEC of indicated
992 JAK2V617F genotype. In these images, N represents the nucleus, white arrows
993 depict rough endoplasmic reticulum, and red arrows showcase accumulated
994 loose ribosomes in mutated iEC. Scale bar, 1,000 nm.

995

996

997

998

999

1000

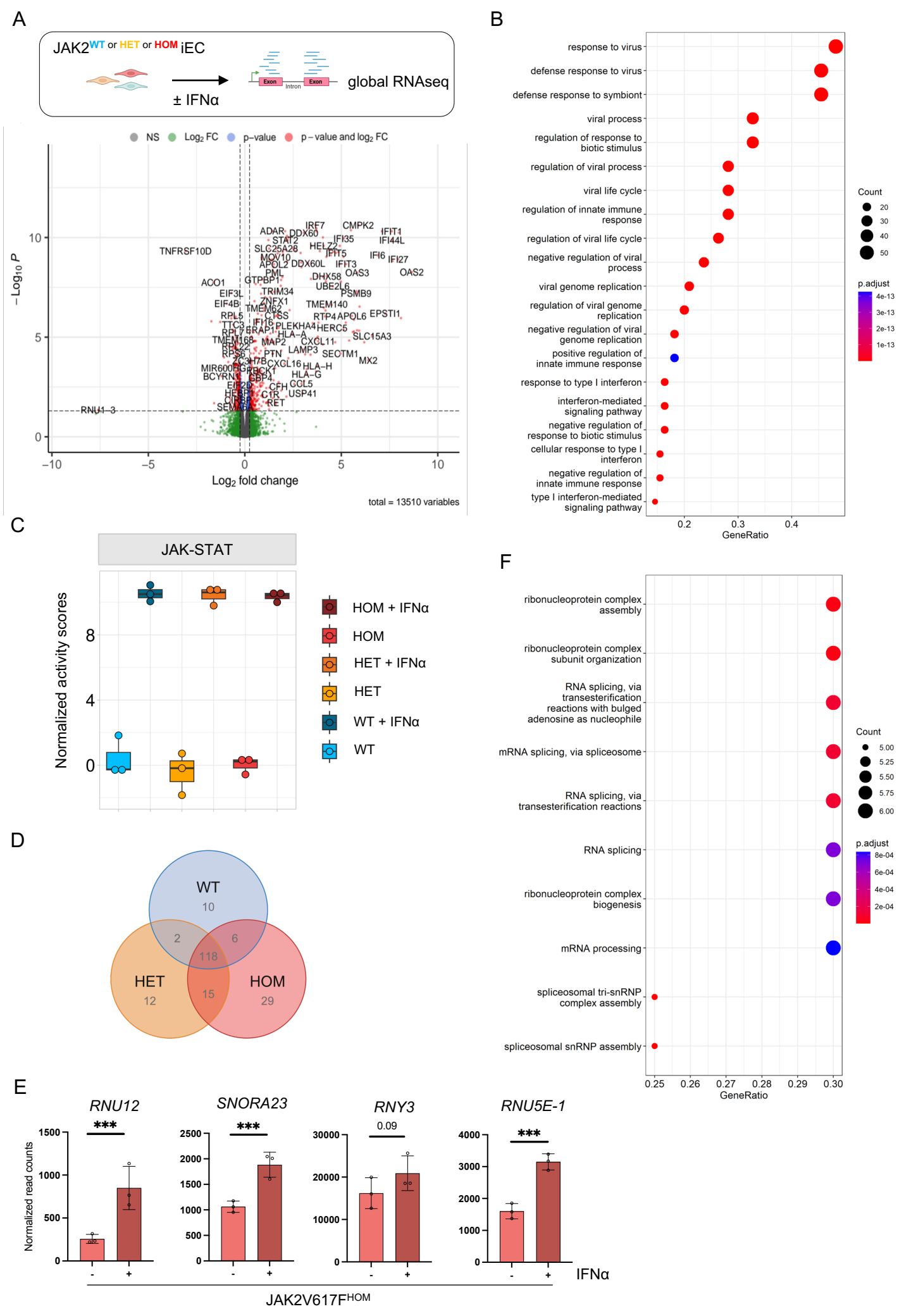
A
JAK2WT or HET or HOM iEC
± IFNα
Exon
Intron
Exon
global RNAseq
NS
Log2 FC
p-value
p-value and log2 FC
−Log10 P
Log2 fold change
total = 13510 variables
B
response to virus
defense response to virus
defense response to symbiont
viral process
regulation of response to biotic stimulus
regulation of viral process
viral life cycle
regulation of innate immune response
regulation of viral life cycle
negative regulation of viral process
viral genome replication
regulation of viral genome replication
negative regulation of viral genome replication
positive regulation of innate immune response
response to type I interferon
interferon-mediated signaling pathway
negative regulation of response to biotic stimulus
cellular response to type I interferon
negative regulation of innate immune response
type I interferon-mediated signaling pathway
GeneRatio
Count
p.adjust
C
JAK-STAT
Normalized activity scores
HOM + IFNα
HOM
HET + IFNα
HET
WT + IFNα
WT
D
WT
10
HET
12
HOM
29
2
6
118
15
E
RNU12
SNORA23
RNY3
RNU5E-1
Normalized read counts
0.09
IFNα
JAK2V617FHOM
F
ribonucleoprotein complex assembly
ribonucleoprotein complex subunit organization
RNA splicing, via transesterification reactions with bulged adenosine as nucleophile
mRNA splicing, via spliceosome
RNA splicing, via transesterification reactions
RNA splicing
ribonucleoprotein complex biogenesis
mRNA processing
spliceosomal tri-snRNP complex assembly
spliceosomal snRNP assembly
GeneRatio
Count
p.adjust

Figure 4. Genotype-Specific Transcriptional Responses of iEC to IFNα Treatment

(A) Volcano plot illustrating differentially expressed genes (DEG) in JAK2^{WT}, JAK2V617F^{HET}, and JAK2V617F^{HOM} iEC following IFNα treatment. Upregulated genes: 168. Downregulated genes: 10. Abbreviations: NS, non-significant; Log2FC: logarithmic fold change.

(B) Gene Ontology (GO) analysis highlighting iEC core IFNα response. The size of the dots reflects the number of dysregulated genes from the gene list associated with the GO term, while the color of the dots represents the adjusted p-value (p. adjust).

(C) Pathway responsive genes (PROGENy) analysis of JAK–STAT pathway activity in iEC following IFNα treatment.

(D) Venn diagram illustrating overlapping and significantly enriched genes within each genotype following IFNα treatment (cut off: adjusted p-value for FDR<0.05). A list of all significantly dysregulated genes is provided in Supplementary Table 9.

(E) Quantification of normalized mRNA read counts for RNA, U12 small nuclear (*RNU12*), Small Nucleolar RNA, H/ACA Box 23 (*SNORA23*), RNA, Y3 (*RNY3*), and RNA, U5E small nuclear 1 (*RNU5E-1*) expression in untreated versus IFNα-treated JAK2V617F^{HOM} iEC (n = 3).

(F) GO analysis depicting upregulated terms in JAK2V617F^{HOM} iEC following IFNα treatment. The size of the dots reflects the number of dysregulated genes from the gene list associated with the GO term, while the color of the dots represents the adjusted p-value (p. adjust).

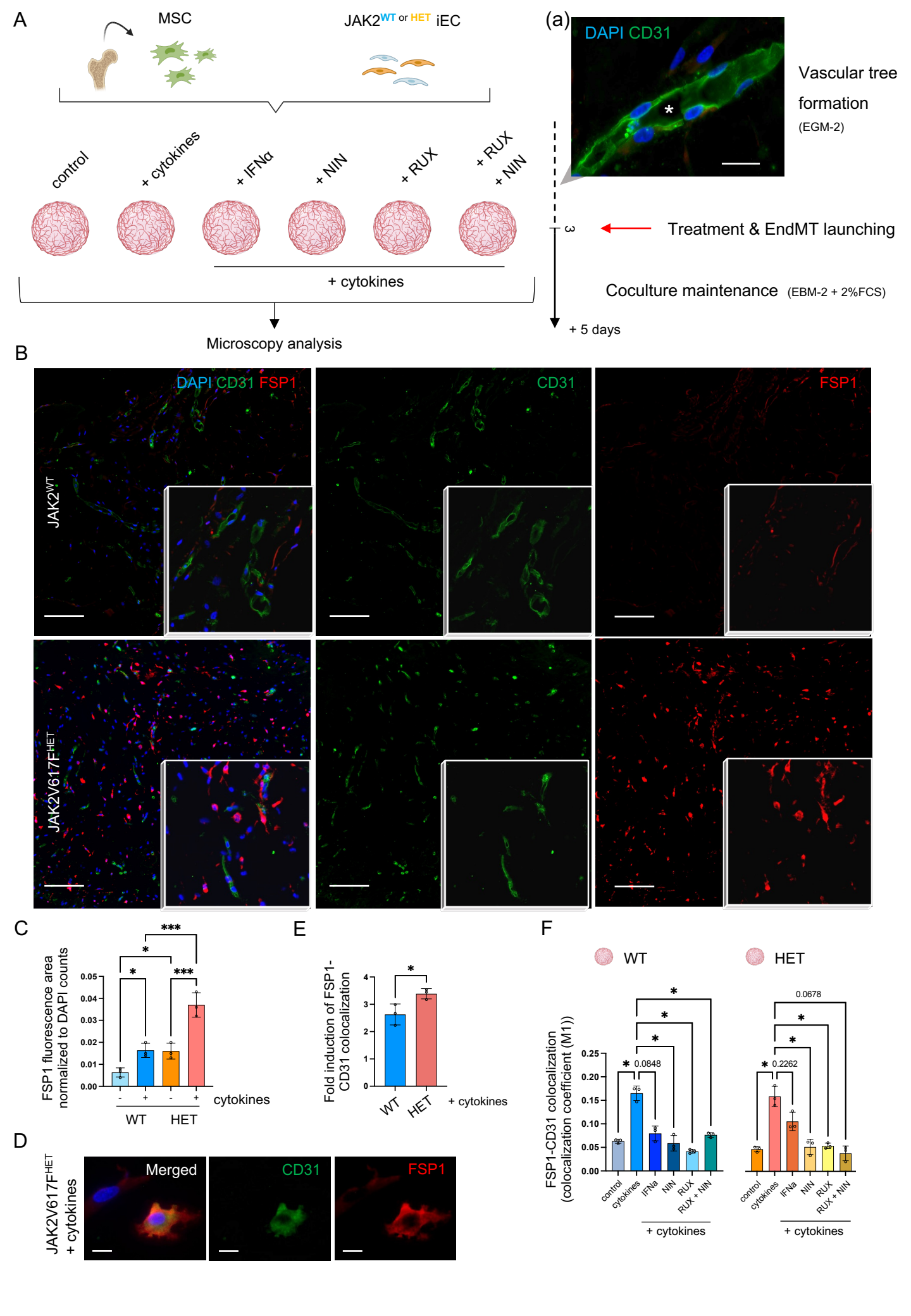
A
MSC
JAK2WT or HET iEC
control
+ cytokines
+ IFNα
+ NIN
+ RUX
+ RUX + NIN
+ cytokines
Microscopy analysis
(a)
DAPI CD31
Vascular tree formation
(EGM-2)
3
Treatment & EndMT launching
Coculture maintenance (EBM-2 + 2%FCS)
+ 5 days
B
DAPI CD31 FSP1
CD31
FSP1
JAK2WT
JAK2V617FHET
C
FSP1 fluorescence area normalized to DAPI counts
cytokines
WT
HET
E
Fold induction of FSP1-CD31 colocalization
WT
HET
+ cytokines
F
WT
HET
FSP1-CD31 colocalization (colocalization coefficient (M1))
0.0848
0.0678
0.2262
control
cytokines
IFNa
NIN
RUX
RUX + NIN
+ cytokines
D
JAK2V617FHET + cytokines
Merged
CD31
FSP1

Figure 5. JAK2V617F-driven EndMT is recapitulated *in vitro* using a 3D iPSC-based model

(A) Schematic representation of the experimental setup. After vascular tree formation, WT and JAK2V617F^{HET} iEC 3D cocultures were pre-treated with IFNα (1000 U/ml), ruxolitinib (RUX, 250 nM), nintedanib (NIN, 250 nM), or a combination of ruxolitinib and nintedanib (both 250 nM). EndMT was then induced using pro-fibrotic cytokines (IL1β, TNFα, and TGFβ) to mimic the pathological conditions of MF. (a) Representative image of 3D coculture stained for CD31 (green) to visualize iEC, with DAPI (blue) highlighting cell nuclei. The asterisk marks a lumen-like structure. Scale bar: 25 µm.

(B) Representative IF images of JAK2^{WT} and JAK2V617F^{HET} 3D cocultures, stained for CD31 (green) and FSP1 (red) to indicate EndMT. Cell nuclei are visualized using DAPI (blue). Scale bar, 125 µm.

(C) Quantification of FSP1 fluorescence area in JAK2^{WT} and JAK2V617F^{HET} 3D cocultures under both stimulated and unstimulated conditions. Two-way ANOVA (n = 3).

(D) Representative duplex IF images showing FSP1 expression in a CD31^{+} iEC following exposure to IL1β, TNFα, and TGFβ in JAK2V617F^{HET} 3D cocultures. Scale bar: 10 µm.

(E) Fold induction of FSP1-CD31 fluorescence colocalization in JAK2^{WT} vs. JAK2V617F^{HET} 3D cocultures after cytokine stimulation. Unpaired t-test (n = 3).

(F) Analysis of FSP1-CD31 fluorescence colocalization under different treatment conditions, quantified using Mander's colocalization coefficient (M1), in JAK2^{WT} and JAK2V617F^{HET} 3D cocultures. One-way ANOVA (n = 3).

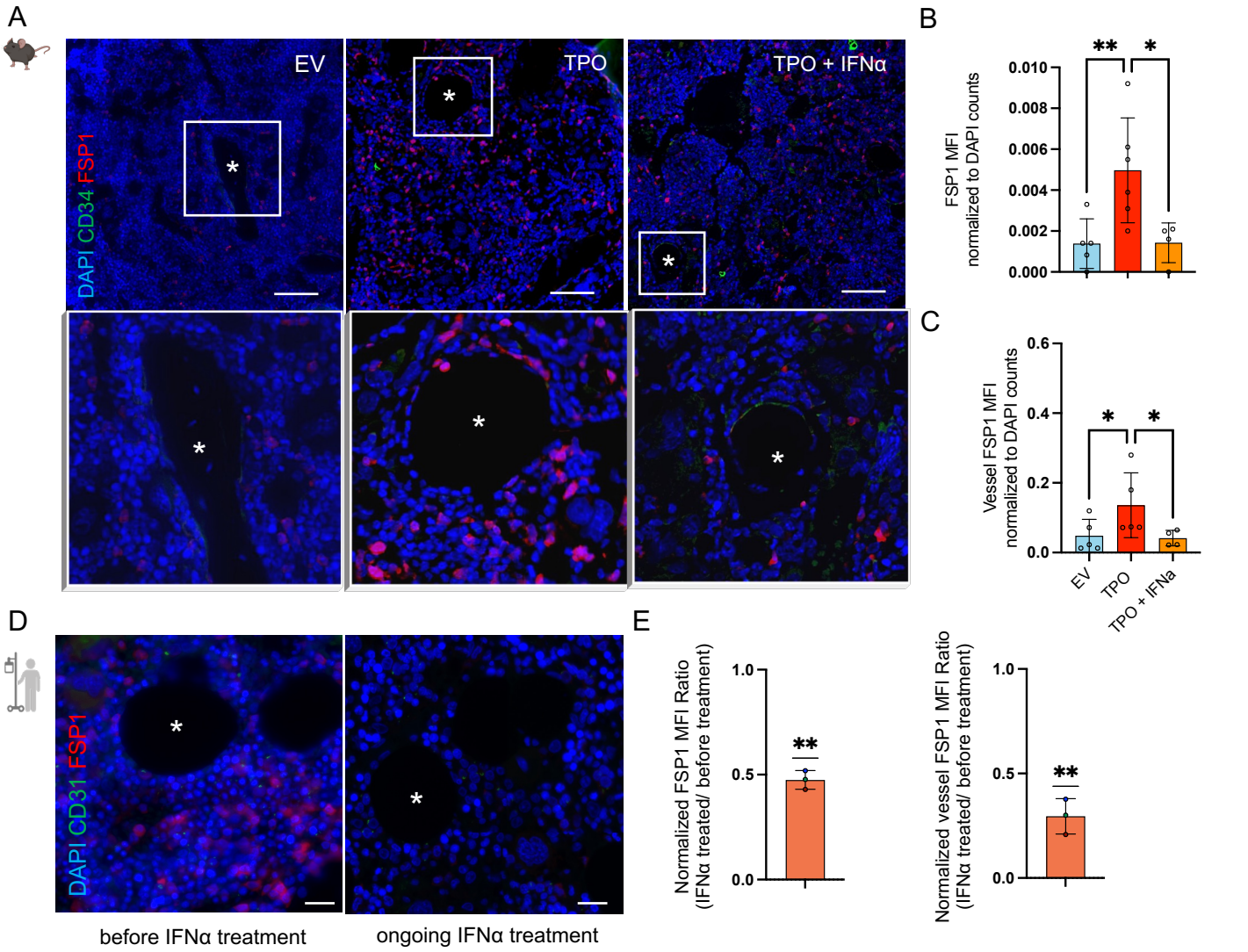
A
EV
TPO
TPO + IFNα
DAPI CD34 FSP1
B
FSP1 MFI
normalized to DAPI counts
0.010
0.008
0.006
0.004
0.002
0.000
**
*
C
Vessel FSP1 MFI
normalized to DAPI counts
0.6
0.4
0.2
0.0
*
*
EV
TPO
TPO + IFNa
D
DAPI CD31 FSP1
before IFNα treatment
ongoing IFNα treatment
E
Normalized FSP1 MFI Ratio
(IFNα treated/ before treatment)
1.0
0.5
0.0
**
Normalized vessel FSP1 MFI Ratio
(IFNα treated/ before treatment)
1.0
0.5
0.0
**

Figure 6. IFNα inhibits EndMT *in vivo*

(A) Representative IF images of BM sections derived from vehicle (EV) and transgenic mice overexpressing thrombopoietin (TPO), treated or not with IFNα over a 4-week period. Sections are co-stained for CD34 (green) and the EndMT marker FSP1 (red), with DAPI (blue) highlighting cell nuclei. Asterisks mark representative vessel lumens. Scale bars: 75 µm.

(B) Global FSP1 mean fluorescence intensity (MFI) quantification. Two-way ANOVA (n = 4-6).

(C) CD34+ vessel-specific FSP1 MFI quantification. Two-way ANOVA (n = 4-6).

(D) Representative IF images of BM sections from MPN patients treated with IFNα. Co-staining shows CD31 (green), FSP1 (red), and nuclei (blue). Asterisks mark vessel lumens. Scale bars, 20 µm.

(E) Normalized ratio of global and $CD31^{+}$ vessel-specific FSP1 MFI during IFNα treatment relative to baseline in MPN patients. Statistical analysis was performed using a one-sample t-test (n = 3). Patient characteristics are detailed in the supplementary information.

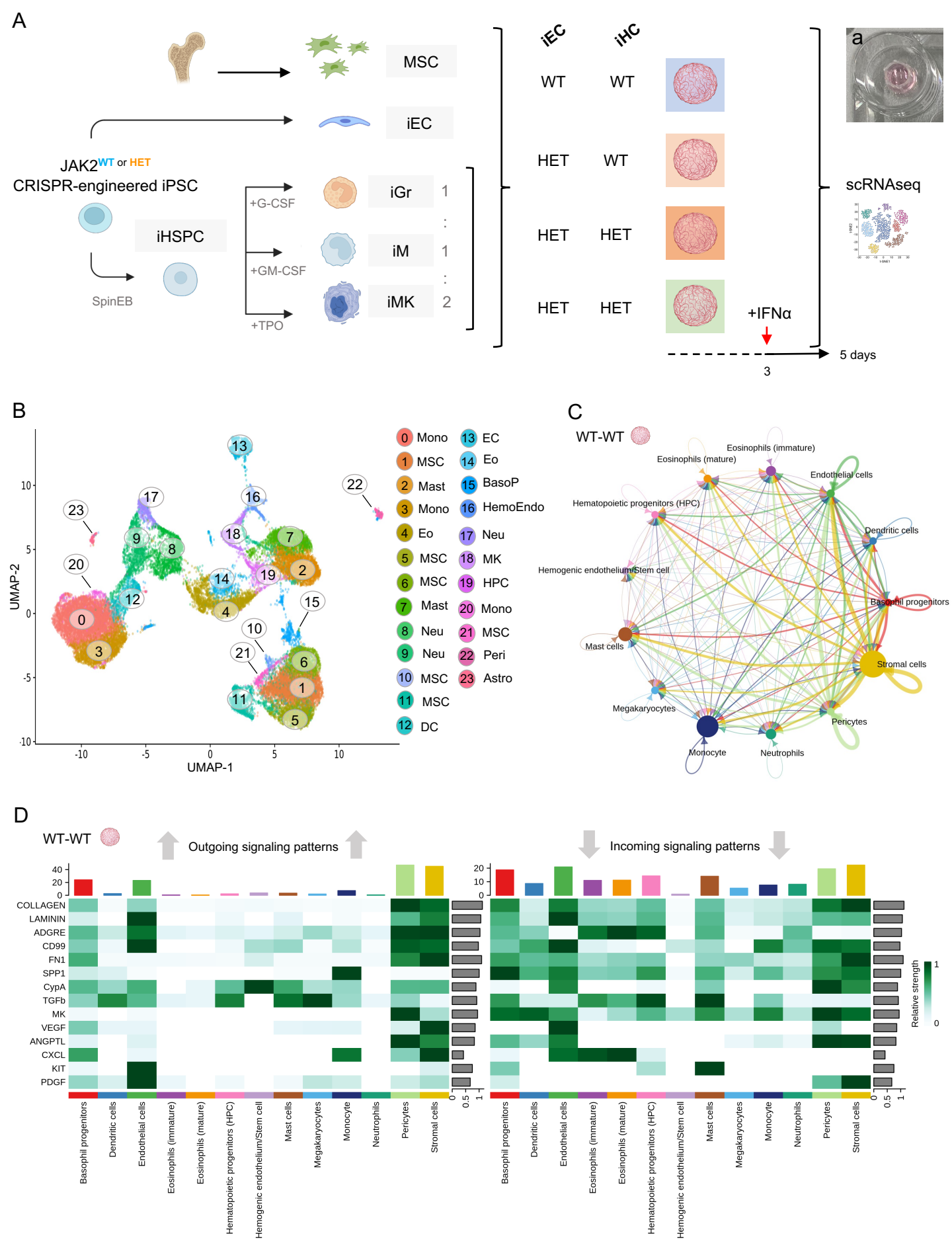
A
MSC
iEC
JAK2WT or HET
CRISPR-engineered iPSC
iHSPC
SpinEB
+G-CSF
+GM-CSF
+TPO
iGr
iM
iMK
1 : 1 : 2
iEC
iHC
WT WT
HET WT
HET HET
HET HET
+IFNα
5 days
3
a
scRNAseq
B
UMAP-1
UMAP-2
0 Mono
1 MSC
2 Mast
3 Mono
4 Eo
5 MSC
6 MSC
7 Mast
8 Neu
9 Neu
10 MSC
11 MSC
12 DC
13 EC
14 Eo
15 BasoP
16 HemoEndo
17 Neu
18 MK
19 HPC
20 Mono
21 MSC
22 Peri
23 Astro
C
WT-WT
Eosinophils (immature)
Eosinophils (mature)
Endothelial cells
Hematopoietic progenitors (HPC)
Dendritic cells
Hemogenic endothelium/Stem cell
Basophil progenitors
Mast cells
Stromal cells
Megakaryocytes
Pericytes
Monocyte
Neutrophils
D
WT-WT
Outgoing signaling patterns
Incoming signaling patterns
COLLAGEN
LAMININ
ADGRE
CD99
FN1
SPP1
CypA
TGFb
MK
VEGF
ANGPTL
CXCL
KIT
PDGF
Relative strength
Basophil progenitors
Dendritic cells
Endothelial cells
Eosinophils (immature)
Eosinophils (mature)
Hematopoietic progenitors (HPC)
Hemogenic endothelium/Stem cell
Mast cells
Megakaryocytes
Monocyte
Neutrophils
Pericytes
Stromal cells

Figure 7. 3D complex cocultures of iEC, iHC, and MSC resume key cellular interactions of the human BM niche

(A) Schematic of the experimental setup for the generation of 3D cocultures for scRNAseq. JAK2^{WT} or JAK2V617F^{HET} iPSC-derived megakaryocytes (iMK), monocytes/macrophages (iM), and granulocytes (iGr) (collectively referred to as iPSC-derived hematopoietic cells (iHC)) were mixed in a 2:1:1 ratio and combined with MSC and JAK2^{WT} or JAK2V617F^{HET} iEC within fibrin hydrogels. To evaluate the effect of IFNα on the mutant niche, JAK2V617F^{HET} cocultures were treated with IFNα (1000 U/ml) for 48h before scRNAseq. (a) Representative photograph of a 3D iPSC-based construct.

(B) Uniform Manifold Approximation and Projection (UMAP) plot showing the isolated hematopoietic and stromal clusters. Abbreviations: Mono – monocytes; MSC – mesenchymal stromal cells; Mast – mast cells; Eo – eosinophils; Neu – neutrophils; DC – dendritic cells; EC – endothelial cells; BasoP – basophil progenitors; HemoEndo – hemogenic endothelium; MK – megakaryocytes; HPC – hematopoietic progenitor cells; Peri – pericytes; Astro – astrocytes.

(C) Circle plot depicting the mapping of ligand-receptor (L-R) interactions among various cell types in JAK2^{WT} (WT-WT) cocultures. Each node represents a distinct cell type, with MSC clusters categorized as stromal cells. Line thickness indicates interaction strength, while arrows denote the direction of the interactions.

(D) Heatmap illustrating the relative strength of incoming and outgoing signaling among various cell types in JAK2^{WT} complex cocultures. Rows represent aggregate strength of signaling for the given pathway, while columns indicate distinct cell types. The color code reflects the strength of the interactions.

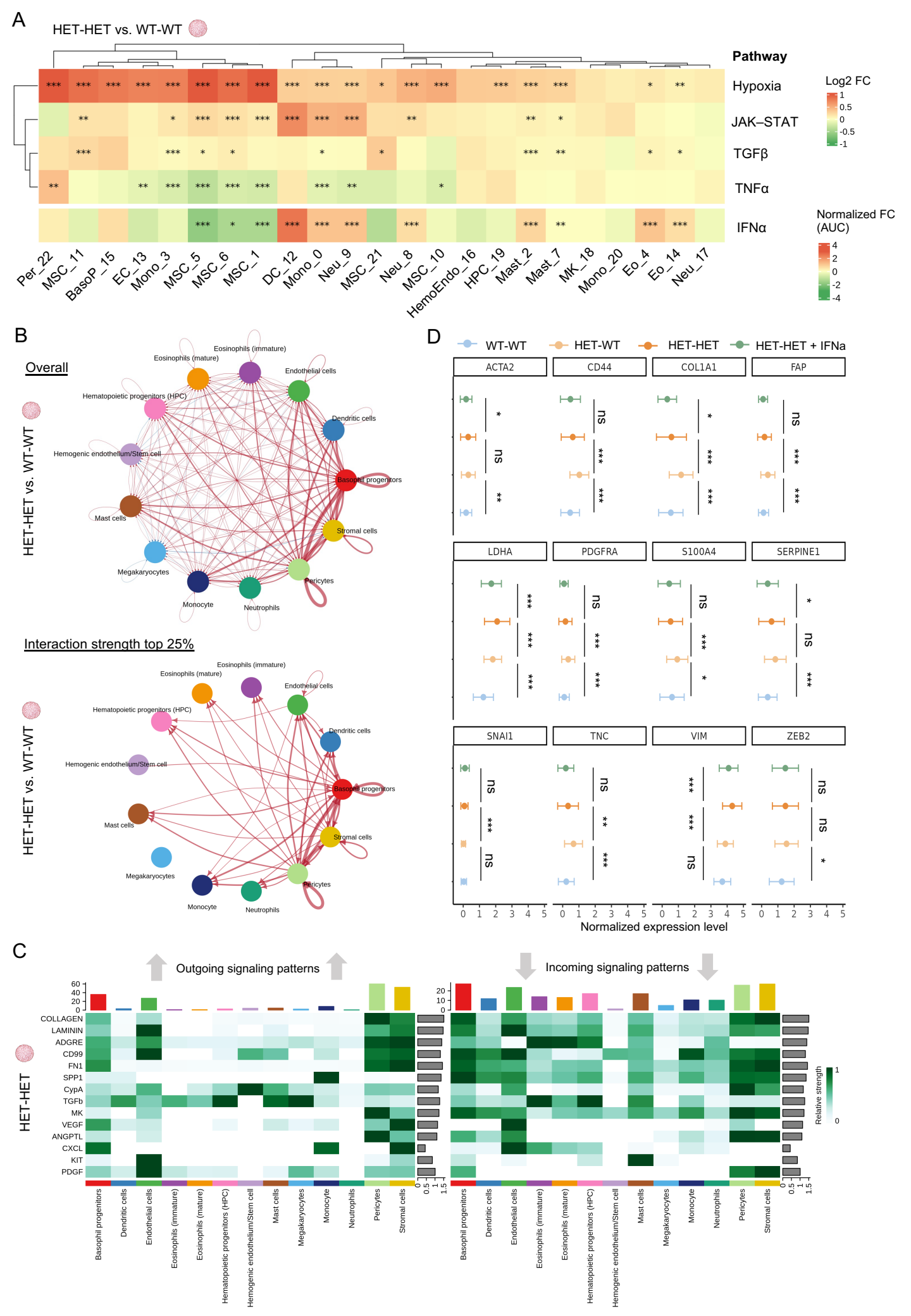
A
HET-HET vs. WT-WT
Pathway
Hypoxia
JAK–STAT
TGFβ
TNFα
IFNα
Log2 FC
Normalized FC (AUC)
Per_22
MSC_11
BasoP_15
EC_13
Mono_3
MSC_5
MSC_6
MSC_1
DC_12
Mono_0
Neu_9
MSC_21
Neu_8
MSC_10
HemoEndo_16
HPC_19
Mast_2
Mast_7
MK_18
Mono_20
Eo_4
Eo_14
Neu_17
B
Overall
HET-HET vs. WT-WT
Eosinophils (mature)
Eosinophils (immature)
Endothelial cells
Hematopoietic progenitors (HPC)
Dendritic cells
Hemogenic endothelium/Stem cell
Basophil progenitors
Mast cells
Stromal cells
Megakaryocytes
Pericytes
Monocyte
Neutrophils
Interaction strength top 25%
HET-HET vs. WT-WT
Eosinophils (mature)
Eosinophils (immature)
Endothelial cells
Hematopoietic progenitors (HPC)
Dendritic cells
Hemogenic endothelium/Stem cell
Basophil progenitors
Mast cells
Stromal cells
Megakaryocytes
Pericytes
Monocyte
Neutrophils
D
WT-WT
HET-WT
HET-HET
HET-HET + IFNa
ACTA2
CD44
COL1A1
FAP
LDHA
PDGFRA
S100A4
SERPINE1
SNAI1
TNC
VIM
ZEB2
Normalized expression level
C
Outgoing signaling patterns
Incoming signaling patterns
HET-HET
COLLAGEN
LAMININ
ADGRE
CD99
FN1
SPP1
CypA
TGFb
MK
VEGF
ANGPTL
CXCL
KIT
PDGF
Relative strength
Basophil progenitors
Dendritic cells
Endothelial cells
Eosinophils (immature)
Eosinophils (mature)
Hematopoietic progenitors (HPC)
Hemogenic endothelium/Stem cell
Mast cells
Megakaryocytes
Monocyte
Neutrophils
Pericytes
Stromal cells

Figure 8. JAK2V617F^{HET} 3D complex cocultures recapitulate key MPN features

(A) PROGENy analysis and Area Under the Curve (AUC) score analysis of selected pathways in JAK2V617F^{HET} cocultures compared to JAK2^{WT} controls. Abbreviations: FC – Fold change of HET-HET vs. WT-WT cocultures.

(B) Circle plot illustrating the overall and top 25% of ligand-receptor (L-R) interaction strength among various cell types in JAK2V617F^{HET} cocultures (HET-HET) versus JAK2^{WT} controls (WT-WT). Each node represents a distinct cell type, with MSC clusters classified as stromal cells. Line thickness reflects interaction strength, and arrows indicate the direction of interactions. Red lines indicate increased interaction strength, while blue lines denote decreased interaction strength.

(C) Heatmap illustrating the relative strength of incoming and outgoing signaling among various cell types in JAK2V617F^{HET} cocultures. Rows represent aggregate strength of signaling for the given pathway, while columns indicate distinct cell types. The color code reflects the strength of the interactions.

(D) Dot plots with error bars showing the normalized expression levels of selected EndMT markers in EC from complex cocultures under different genetic backgrounds and treatment conditions. Color codes represent the investigated conditions: **blue** for JAK2^{WT} iEC-iHC cocultures, **yellow** for JAK2V617F^{HET} iEC-JAK2^{WT} iHC cocultures, **orange** for JAK2V617F^{HET} iEC-iHC cocultures, and **green** for JAK2V617F^{HET} iEC-iHC cocultures treated with IFNα (1000 U/ml) for 48 hours prior to scRNA-seq.

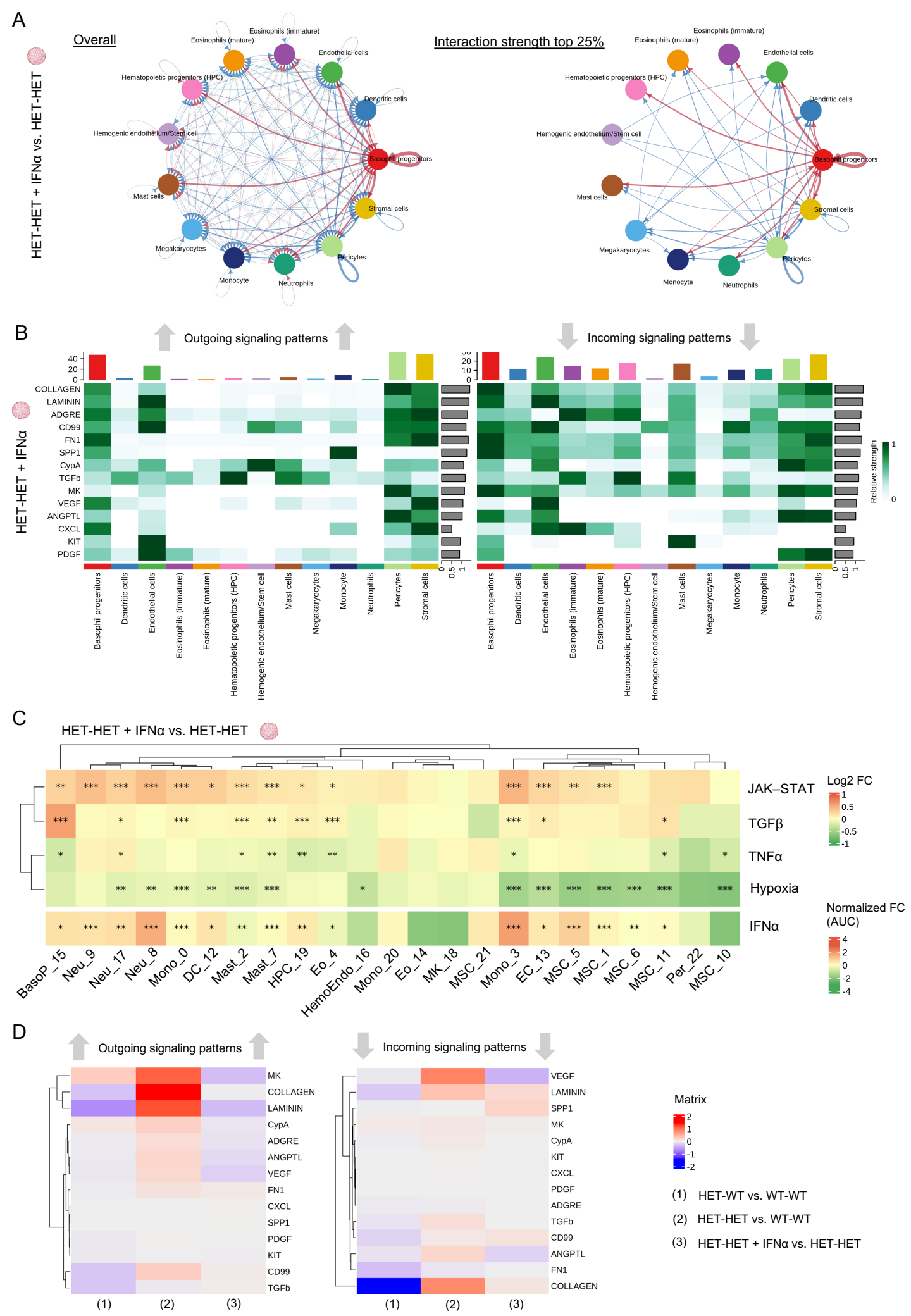
A
Overall
Interaction strength top 25%
HET-HET + IFNα vs. HET-HET
Eosinophils (immature)
Eosinophils (mature)
Endothelial cells
Hematopoietic progenitors (HPC)
Dendritic cells
Hemogenic endothelium/Stem cell
Basophil progenitors
Mast cells
Stromal cells
Megakaryocytes
Pericytes
Monocyte
Neutrophils
B
Outgoing signaling patterns
Incoming signaling patterns
HET-HET + IFNα
COLLAGEN
LAMININ
ADGRE
CD99
FN1
SPP1
CypA
TGFb
MK
VEGF
ANGPTL
CXCL
KIT
PDGF
Relative strength
C
HET-HET + IFNα vs. HET-HET
JAK–STAT
TGFβ
TNFα
Hypoxia
IFNα
Log2 FC
Normalized FC (AUC)
BasoP_15
Neu_9
Neu_17
Neu_8
Mono_0
DC_12
Mast_2
Mast_7
HPC_19
Eo_4
HemoEndo_16
Mono_20
Eo_14
MK_18
MSC_21
Mono_3
EC_13
MSC_5
MSC_1
MSC_6
MSC_11
Per_22
MSC_10
D
Outgoing signaling patterns
Incoming signaling patterns
Matrix
(1) HET-WT vs. WT-WT
(2) HET-HET vs. WT-WT
(3) HET-HET + IFNα vs. HET-HET

Figure 9. IFNα mitigates pro-fibrotic signaling in 3D JAK2V617F^{HET} complex cocultures

(A) Circle plot illustrating the overall and top 25% of ligand-receptor (L-R) interaction strength among various cell types in cocultures treated with 1000 U/ml IFNα (HET-HET + IFNα) compared to JAK2V617F^{HET} cocultures (HET-HET). Each node represents a distinct cell type, with MSC clusters classified as stromal cells. Line thickness reflects interaction strength, and arrows indicate the direction of interactions. Red lines represent increased interaction strength, while blue lines indicate decreased interaction strength.

(B) Heatmap illustrating the relative strength of incoming and outgoing signaling among various cell types in JAK2V617F^{HET} cocultures treated with IFNα. Rows represent aggregate strength of signaling for the given pathway, while columns indicate distinct cell types. The color code reflects the strength of the interactions.

(C) PROGENy analysis and AUC score analysis of selected pathways in JAK2V617F^{HET} cocultures treated with IFNα (HET-HET + IFNα) compared to untreated JAK2V617F^{HET} cocultures (HET-HET). Abbreviations: FC – Fold change of HET-HET + IFNα vs. HET-HET cocultures.

(D) Heatmap comparing incoming and outgoing signaling in iEC based on ligand-receptor (L-R) analysis from scRNAseq experiment. The columns represent the tested conditions: (1) HET-WT vs. WT-WT, (2) HET-HET vs. WT-WT, and (3) HET-HET + IFNα vs. HET-HET. Each row corresponds to a mediator of interaction. The color gradient from red to blue indicates increasing to decreasing interaction strength mediated by the listed factors.